Title
Fragment-based Differential Targeting of PPI Stabilizer Interfaces

Journal
Journal of Medicinal Chemistry, 63(13)

ISSN
0022-2623

Authors
Guillory, Xavier
Wolter, Madita
Leysen, Seppe
et al.

Publication Date
2020-07-09

DOI
10.1021/acs.jmedchem.9b01942

Peer reviewed

Journal of Medicinal Chemistry

pubs.acs.org/jmc

Article

Fragment-based Differential Targeting of PPI Stabilizer Interfaces

Xavier Guillory, Madita Wolter, Seppe Leysen, João Filipe Neves, Ave Kuusk, Sylvia Genet, Bente Somsen, John Kenneth Morrow, Emma Rivers, Lotte van Beek, Joe Patel, Robert Goodnow, Heike Schoenherr, Nathan Fuller, Qing Cao, Richard G. Doveston, Luc Brunsveld, Michelle R. Arkin, Paola Castaldi, Helen Boyd, Isabelle Landrieu,* Hongming Chen,* and Christian Ottmann*

Cite This: *J. Med. Chem.* 2020, 63, 6694–6707

Read Online

ACCESS | Metrics & More | Article Recommendations | Supporting Information

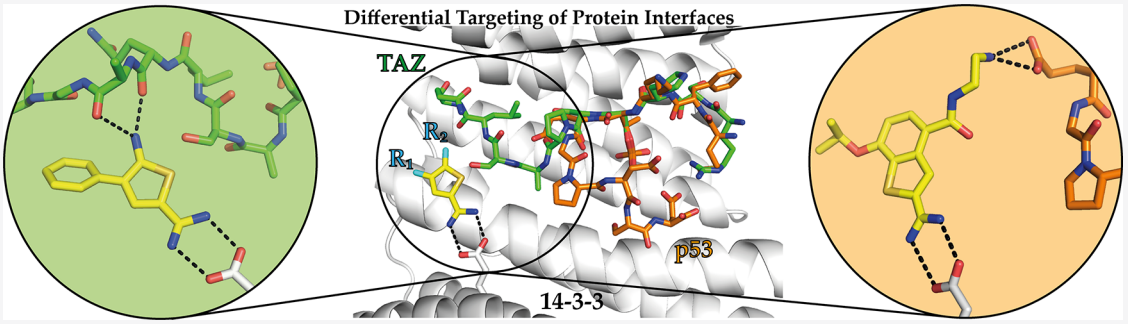

ABSTRACT: Stabilization of protein−protein interactions (PPIs) holds great potential for therapeutic agents, as illustrated by the successful drugs rapamycin and lenalidomide. However, how such interface-binding molecules can be created in a rational, bottom-up manner is a largely unanswered question. We report here how a fragment-based approach can be used to identify chemical starting points for the development of small-molecule stabilizers that differentiate between two different PPI interfaces of the adapter protein 14-3-3. The fragments discriminately bind to the interface of 14-3-3 with the recognition motif of either the tumor suppressor protein p53 or the oncogenic transcription factor TAZ. This X-ray crystallography driven study shows that the rim of the interface of individual 14-3-3 complexes can be targeted in a differential manner with fragments that represent promising starting points for the development of specific 14-3-3 PPI stabilizers.

INTRODUCTION

PPI modulation is one of the most promising and active fields in current drug discovery and chemical biology.[1] However, PPI modulation is in many instances understood synonymously with PPI inhibition, disregarding the complementary strategy of stabilizing PPIs. This is despite the fact that a multitude of natural products[2] and a growing number of synthetic compounds[3] validate the feasibility and value of small-molecule PPI stabilization. Stabilizers of PPIs display a number of advantages like their uncompetitive nature and their potential for higher specificity. They bind to composite pockets at the interface of their target protein complexes that naturally can show a much higher structural variability compared for example to active sites of enzymes or ligand binding pockets of receptors. Consequently, the potential to develop selective PPI-stabilizing compounds might be higher than with ligands that bind to conventional drug targets. An especially interesting target for PPI modulation is the adapter protein 14-3-3. This "hub" protein, consisting of a family of seven isoforms, interacts with several hundred partner proteins[4] and regulates the activity of many disease-related proteins like C-Raf[5−7] (cancer), Tau[8,9] (Alzheimer's), and CFTR[10,11] (cystic fibrosis).

Here, we focused on the interaction of 14-3-3 with the transcriptional coactivator TAZ and the tumor suppressor protein p53. TAZ interacts with 14-3-3 via a motif surrounding S89, which, as part of the Hippo signaling pathway, is phosphorylated by LATS1/2, resulting in cytoplasmic retention of TAZ and thus its functional deactivation.[12] Loss of this regulation leads to abrogation of contact inhibition, which is one of the prerequisites of cancer formation and growth of solid tumors. Binding of 14-3-3 to p53, following phosphorylation of T387 of p53 in response to DNA damage, is protective against MDM2-mediated degradation.[13] In addition, 14-3-3 binding to p53 facilitates p53 dimer−dimer interaction[14] and stabilization of the functional p53 tetramer.[15]

Received: November 25, 2019
Published: June 5, 2020

https://dx.doi.org/10.1021/acs.jmedchem.9b01942
J. Med. Chem. 2020, 63, 6694−6707

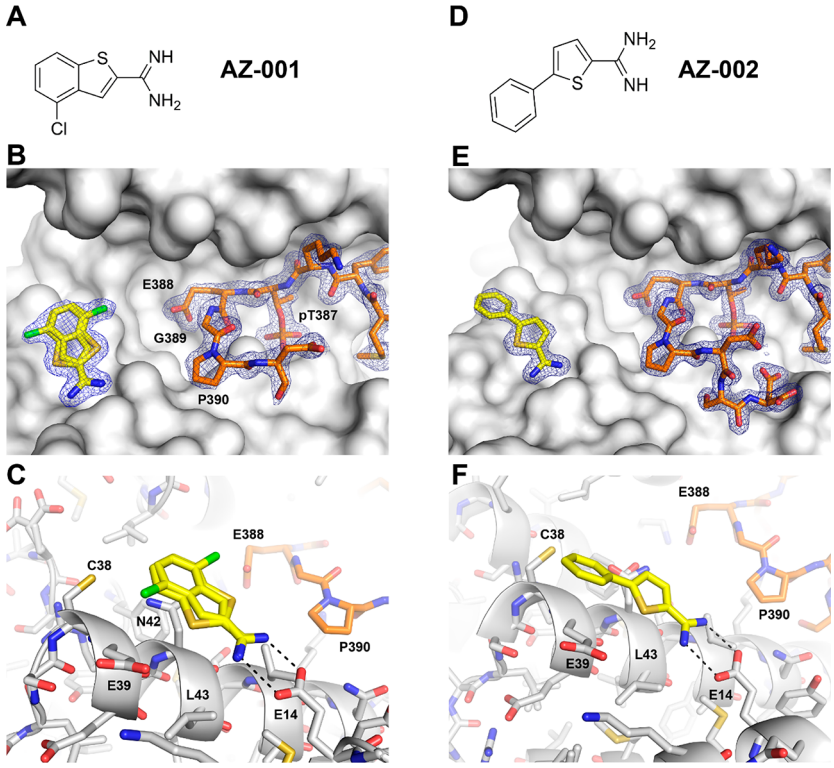

Figure 1. Identification of fragments binding to the interface of 14-3-3σ with p53. (A) Fragment AZ-001. (B) Crystal structure of AZ-001 (yellow sticks) in complex with 14-3-3σ (white surface) and p53pT387 (orange sticks), PDB 6S40. The final $2F_o - F_c$ electron density maps are shown as blue mesh. (C) Detailed view of the binding pocket of AZ-001. The most prominent interaction is a salt-bridge (dotted black line) between the amidine of AZ-001 and carboxyl group of E14 of 14-3-3σ. (D) Fragment AZ-002. (E) Crystal structure of AZ-002 (yellow sticks) in complex with 14-3-3σ (white surface) and p53pT387 (orange sticks), PDB 6RWI. The final $2F_o - F_c$ electron density maps are shown as blue mesh. (F) Detailed view of the binding pocket of AZ-002. Also with AZ-002, the most prominent interaction is a salt-bridge (dotted black line) between the amidine of AZ-002 and carboxyl group of E14 of 14-3-3σ.

14-3-3 thus plays an important role in maintaining the tumor suppressor role of p53 by stimulating p53's transcriptional activity. Enhancing the binding of 14-3-3 to these two cancer-related proteins with a small-molecule 14-3-3 PPI stabilizer could convey a positive therapeutic effect in many cancer types.

Importantly, the potential "druggability" of 14-3-3 proteins has been validated by nature in the form of the natural products class of the fusicoccanes. These diterpene glycosides have been shown to stabilize a number of 14-3-3 PPIs and display biological activities that might be of therapeutic benefit in cancer,[5,16−20] cystic fibrosis,[10,11,21] and axon regeneration.[22] The eponymous molecule, the fungal toxin fusicoccin A (FC-A), was shown to stabilize the interaction of 14-3-3 proteins with the regulatory C-terminus of the plant plasma ATPase, thereby activating this important proton pump.[23] Later it was shown that the related compound cotylenin A displays a remarkable anticancer activity while showing a very low general toxicity.[24] One possible target for this activity was suggested by us to be the negative regulatory complex between the N-terminus of the oncogenic kinase C-Raf and 14-3-3 proteins.[7] The crystal structure of cotylenin A in complex with 14-3-3ζ and the diphospho peptide C-RafpS233pS259 showed that the natural product binds to a gap in the interface pocket simultaneously, establishing contacts to both 14-3-3 and the C-Raf-derived peptide. Recently, an optimized semisynthetic fusicoccane was shown to display enhanced antiproliferative activity against cancer cells.[25] Furthermore, we reported that the natural product FC-A displayed a beneficial effect for a potential therapy of breast cancer and cystic fibrosis by stabilizing the inhibitory interaction of 14-3-3 with estrogen receptor α[26] or the chloride channel CFTR.[11] Although the fusicoccanes are very useful proof-of-principle molecules, their optimization is not without synthetic challenges. Therefore, additional approaches to identify starting points for the development of PPI stabilizers are needed. Because traditional high throughput-screening (HTS) were so far rewarded with only limited success,[27] alternative methods like fragment-based drug discovery (FBDD) holds the most promise to achieve this goal.

In this study, we report the identification of fragments that bind to the distinct interfaces of 14-3-3 with the partner proteins p53 and TAZ, hinting at the possibility to introduce specificity at an early stage of fragment-based optimization of 14-3-3 PPI stabilizing ligands.

RESULTS

Screening for Fragments That Bind to the Interface of 14-3-3 with TAZ and p53. For the identification of interface-binding fragments that might be developed into PPI-stabilizing compounds, we employed a crystallography-based screen of fragment cocktails.[28] Here, crystals of the binary 14-3-3 complexes were soaked in solutions of fragment mixtures (100 cocktails of five each, part of the X-ray crystallography subset of the AstraZeneca fragments collection) at a final concentration of 10 mM per fragment. This screen identified two scaffolds that bound to a shallow pocket that is located in the central binding channel of 14-3-3. Both fragment scaffolds

https://dx.doi.org/10.1021/acs.jmedchem.9b01942
J. Med. Chem. 2020, 63, 6694−6707

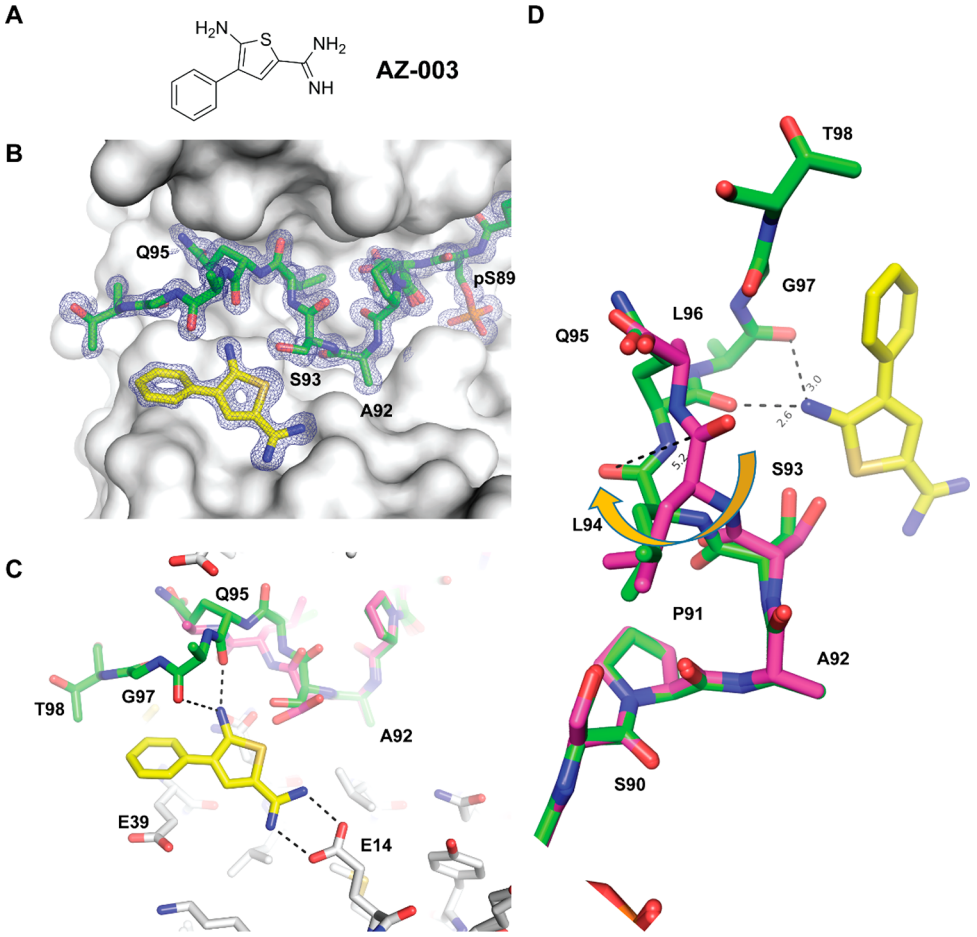

Figure 2. AZ-003 bound to 14-3-3σ/TAZpS89. (A) Structure of fragment AZ-003. (B) Crystal structure of AZ-003 (yellow sticks) bound to the complex of 14-3-3σ (white surface) and TAZpS89 (green sticks), PDB 6RLH. The final $2F_o - F_c$ electron density maps are shown as blue mesh. (C) Contacts between AZ-003, 14-3-3σ, and TAZpS89. The structure of TAZpS89 bound to 14-3-3σ in the absence of AZ-003 is superimposed as magenta sticks. (D) Details of the changes binding of AZ-003 induces in the conformation of the TAZpS89 peptide. The peptide backbone flip is indicated by an orange arrow, and the distance between the positions of the main-chain carbonyl oxygen is shown. Polar contacts between the amino group of AZ-003 and main-chain carbonyls of TAZpS89 are indicated as dotted, black lines.

contain an amidine group (Figure 1A,D) that engages in a salt-bridge with the side chain carboxyl group of glutamic acid 14 (E14) of 14-3-3 (Figure 1C,F). The planar aromatic ring systems sit in a shallow pocket that is comprised of 14-3-3 residues E39, N42, and L43 (Figure 1C). The first fragment (AZ-001) can adopt two orientations with the chloride substituent either pointing toward or away from the peptide-binding channel of 14-3-3. The second fragment (AZ-002) shows a more defined orientation, with the benzyl substituent of the thiophene ring pointing away from the peptide, resting on an uncharged cushion comprised by the hydrocarbon part of C38 and E39 of helix 3 of 14-3-3. Structural analogues of AZ-002, namely AZ-003 and AZ-004, were additionally selected from the screen and observed to bind to 14-3-3 in the presence of the p53pT387 but not contacting the peptide (Supporting Information (SI), Figures S1−S2).

AZ-003 Interacts with Both 14-3-3 and TAZ and Induces a Conformational Change in the TAZpS89 Peptide. In contrast to the 14-3-3/p53pT387 complex, the binding site of AZ-003 lies directly at the interface of 14-3-3 with the TAZpS89 peptide (Figure 2A,B). When this fragment was soaked into crystals of the binary complex, we observed a significant change in the conformation of the TAZ peptide (Figure 2C,D). Most obvious is the additional electron density at the C-terminus of the peptide, which allowed us to build three additional amino acids (L96-T98). Second, a peptide flip is observed between L94 and Q95 which allows the main chain carbonyl oxygen of Q95 to establish a polar contact with the amine group of AZ-003 (Figure 2D). Finally, the carbonyl oxygen of L96 is interacting in the same manner with this amine substituent. It is likely that these interactions are the reason for the observed changes in the conformation of the TAZ peptide because the similar structural analogue of AZ-004 does not invoke comparable structural differences (SI, Figure S3). Complementary protein-based NMR experiments allowed us to confirm the binding site of AZ-003 to 14-3-3σ and to the 14-3-3σ/TAZpS89 complex in solution (SI, Figures S4, S5). Further characterization of the effect of AZ-003 on the binary complex using fluorescence polarization (SI, Figure S6) revealed an increase in anisotropy in the control experiment (no protein), a sign of interferences which make this assay unsuitable for this particular fragment. Even though a stabilizing activity could not be confirmed by FP for AZ-003, based on the observed conformational change induced by the newly formed interactions with two residues of TAZpS89, we believe that fragment AZ-003 represents a promising chemical starting point that could be developed into a more potent

https://dx.doi.org/10.1021/acs.jmedchem.9b01942
J. Med. Chem. 2020, 63, 6694−6707

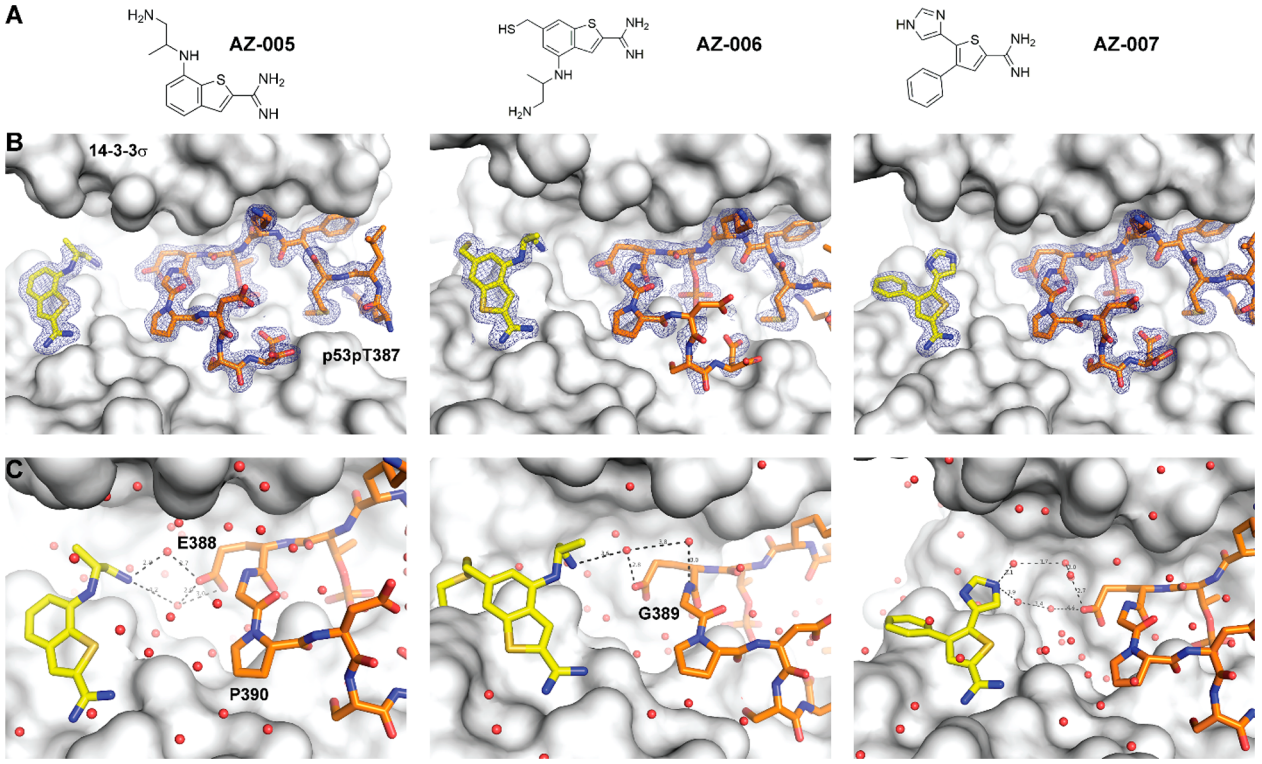

Figure 3. AZ fragments that reach into the water network between 14-3-3σ and p53pT387. (A) Fragments AZ-005, AZ-006, and AZ-007. (B) Crystal structures of the fragments bound to the complex of 14-3-3σ (white surface) and p53pT387 (orange sticks), PDBs 6RX2, 6R5L, and 6RWH, respectively. The final $2F_o - F_c$ electron density maps are shown as blue mesh. (C) Contacts between the fragments and the water network between 14-3-3σ and p53pT387.

orthosteric stabilizer, for example, by modulating the phenyl ring attached to the thiophene C4 position.

Preliminary Fragment Extension Confers Selectivity toward 14-3-3σ in Complex with p53pT387 over TAZpS89. On the basis of the structural data presented, fragments were designed and custom synthesized (SI, Scheme S1−S4), leading to the identification of fragments (Figure 3A) that were compatible with binding to the 14-3-3σ/p53pT387 complex, but not to the 14-3-3σ/TAZpS89 complex. Several structural features of the 14-3-3σ/p53pT387 complex have to be taken into consideration for the prospect of achieving specificity in stabilization. First, the sharp U-turn that the peptide is showing C-terminal of E388 is enabled by the consecutive presence of both a glycine (G389) and a proline (P390). This architecture is further supported by the unique feature that the entire protein ends three amino acids further, with the sequence DSD where both the side chain of the ultimate aspartate and the free C-terminus engage the guanidinium group of R60 in a salt bridge. Together with the rather unusual glutamate at position +1 (E388) after the phosphorylated threonine (pT387), this makes quite a unique interface (Figure 1B,E), which might allow for the development of a specific orthosteric 14-3-3σ/p53pT387 PPI stabilizer. With these requirements in mind, synthesized fragments AZ-005, AZ-006, and AZ-007 (Figure 3A) represent useful chemical starting points for structural optimizations toward p53pT387-specific 14-3-3 PPI stabilizers. The crystal structures of these fragments soaked into binary crystals of 14-3-3σ with the p53 peptide (Figure 3B) showed that the nitrogen-bearing extensions of the core scaffold point toward the p53 peptide and reach into the water network between 14-3-3 and p53 (Figure 3C). Because the TAZ peptide occupies the entire length of the 14-3-3 binding channel, these binding modes are expected to be incompatible with the presence of the TAZ peptide (SI, Figure S7). Consequently, we could not identify additional electron density after soaking these fragments into 14-3-3σ/TAZpS89 crystals, with the exception of AZ-006, which can form a disulfide bond with C38 and is therefore able to compete with TAZpS89 for binding to 14-3-3, resulting in a clear loss of electron density of the TAZ peptide, but of parts of the fragment, too (SI, Figure S8).

AZ-008 Binds to and Shows Weak Stabilization of the 14-3-3/p53pT387 Complex. For the goal of developing an orthosteric PPI stabilizer of the 14-3-3/p53pT387 complex, it seems necessary that an extended fragment based on AZ-005−AZ-007 has to reach the p53 peptide and preferentially engage the side chain of E388. These considerations led to the design of AZ-008 (Figure 4A), which in a docking calculation is predicted to contact the carboxyl group of E388 with its terminal amino group (Figure 4B). We tried to soak this compound into preformed 14-3-3/p53pT387 crystals and also undertook extensive cocrystallization trials, but unfortunately we were not able to detect any additional electron density by X-ray crystallography for compound AZ-008. We thus used WaterLOGSY NMR experiments to detect the potential interaction of AZ-008 to 14-3-3σ. Positive ^{1}H signals of the ligand in the presence of the protein are indicative of binding. Positive NMR signals in the WaterLOGSY spectra of AZ-008 mixed to 14-3-3σ, both in the presence or absence of the p53pT387 peptide, confirmed the interactions (SI, Figure S9). The two-dimensional spectrum (^{1}H−^{15}N TROSY-HSQC) of 14-3-3σ (^{15}N^{2}H labeled) was next used as reporter to further characterize the binding. Because the resonances in this spectrum are sensitive to the chemical environment of the

https://dx.doi.org/10.1021/acs.jmedchem.9b01942
J. Med. Chem. 2020, 63, 6694−6707

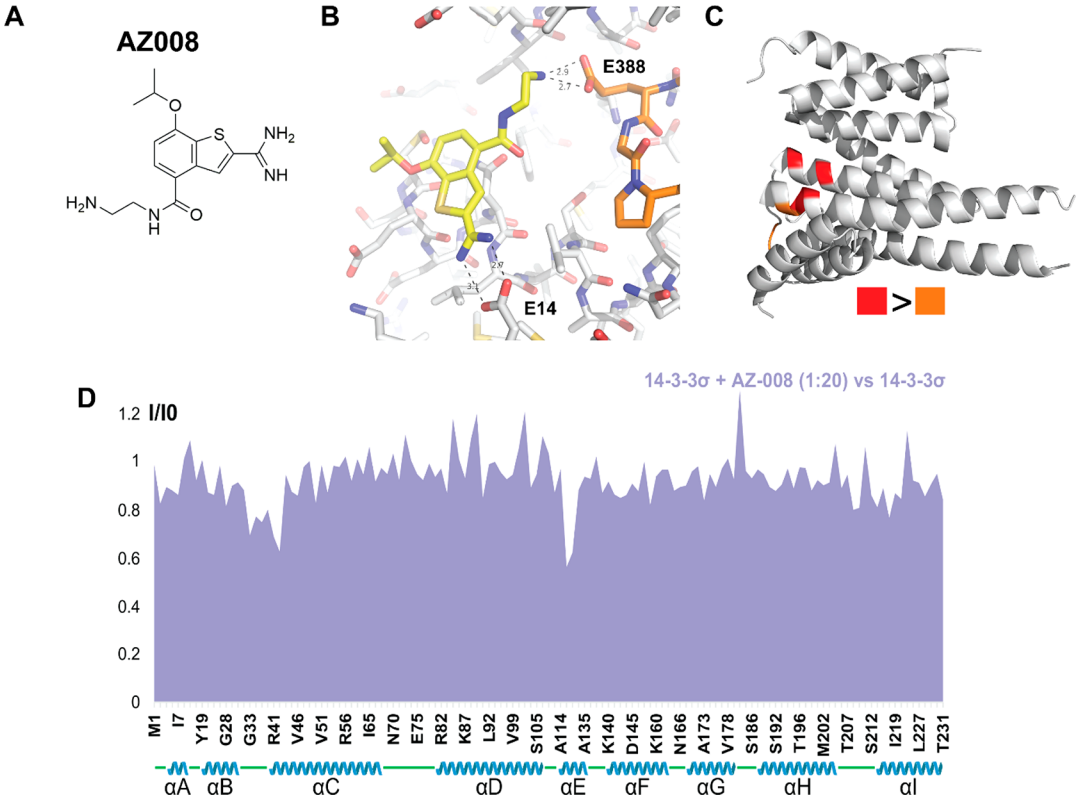

Figure 4. AZ-008 binds to the 14-3-3σ/p53pT387 complex. (A) Structure of AZ-008. (B) Docking of AZ-008 (yellow sticks) bound to the 14-3-3σ (white sticks) in complex with p53pT387 (orange sticks). (C) Mapping on the crystal structure of 14-3-3σ (PDB 1YZ5) of the amino acid residues corresponding to the most affected resonances by the presence of AZ-008. Residues whose corresponding correlation peak intensities were the most affected are colored in red, and an additional 5−8 are colored in brown. (D) Plot of the intensity ratios I/I_0 of corresponding $^{1}H-^{15}N$ correlation peaks in the 2D 14-3-3σ spectra corresponding to the bound 14-3-3σ (100 μM 14-3-3σ in the presence of 2000 μM AZ-008, I) and free 14-3-3σ (100 μM 14-3-3σ I_0) protein (y axis) versus 14-3-3σ amino acid sequence (x axis). A total of 133 correlation peak intensities are shown. The x axis is not proportional to the sequence length. The helices of 14-3-3σ are identified below the x axis as blue cartoons, while disordered regions are represented by green lines.

corresponding residues, a modification in the presence of a ligand of a resonance chemical shift value, and/or intensity, reports an interaction.[29] In addition, chemical shift assignments of 14-3-3σ have been performed, allowing to link a resonance in the spectrum to a specific amino acid residue in the 14-3-3σ sequence. The addition of AZ-008 to 14-3-3σ or 14-3-3σ in the presence of the p53pT387 peptide resulted in detectable broadening (intensity decrease) and chemical shift value perturbation (CSP) of a few resonances in the $^{1}H-^{15}N$ 2D spectrum of the protein (SI, Figures S10−S11, Figures 4C,D, 5A). On the basis of the signal assignments, we concluded that addition of AZ-008 affected mainly the intensity of resonances of residues R41, N42, E115, and F119 of 14-3-3σ (Figure 4C,D, SI, Figure S11A,B), with no variation in the AZ-008 binding pocket mapping in the presence of the p53pT387 peptide (Figures 4D and 5A, and SI, Figure S10). These experiments indicated that binding of AZ-008 occurs in the same pocket in both cases, with or without the p53pT387 peptide. Visualizing the corresponding amino acid perturbation induced by AZ-008 on the 14-3-3σ structure clearly highlighted a binding site (Figure 4C), which can be matched to data from the cocrystal structure of 14-3-3σ and p53pT387 in the presence of its analogues AZ-001/002 (Figure 1). The binding pose resulting from docking AZ-008 to the 14-3-3σ/p53pT387 complex (Figure 4B) is in accordance with both the NMR data and the bound-conformation adopted by other AZ fragments based on this scaffold.

Interestingly, addition of AZ-008 also induced chemical shift perturbations of the ^{1}H NMR signals of the bound peptide (Figure 5B, SI, Figure S12). In particular, the ^{1}H signals (Figure 5B) of the Hδ methyl protons of L383 of the p53pT387 peptide are affected by AZ-008 binding despite the fact that they are not close to the fragment binding site. Perturbation of these signals thus did not correspond to a direct effect due to the local change of environment. This data rather suggests that the binding of the fragment impacted the global binding of the peptide to 14-3-3σ. Moreover, the extent of decrease of the intensity of specific resonances in the 2D spectrum of 14-3-3σ in the presence of AZ-008 reports on the amount of complex present in solution. The intensity of resonances corresponding to amino acid residues located in, or close to, the p53pT387 binding site specifically decreased with the addition of AZ-008 to a solution containing the 14-3-3σ/p53pT387 complex (Figure 5C,D) and, reversely, the extent of CSP increased (SI, Figure S11C). Combined with the results of other methods, this observation indicates that the amount of 14-3-3σ/p53pT387 complex present in solution was increased when both ligands were present, suggesting that the complex was therefore stabilized in the presence of AZ-008. Further experiments using fluorescence polarization (Figure 5E, SI, Figure S13) and surface plasmon resonance (Figure 5F, SI, Figure S14) also suggested that AZ-008 is able to stabilize the

https://dx.doi.org/10.1021/acs.jmedchem.9b01942
J. Med. Chem. 2020, 63, 6694−6707

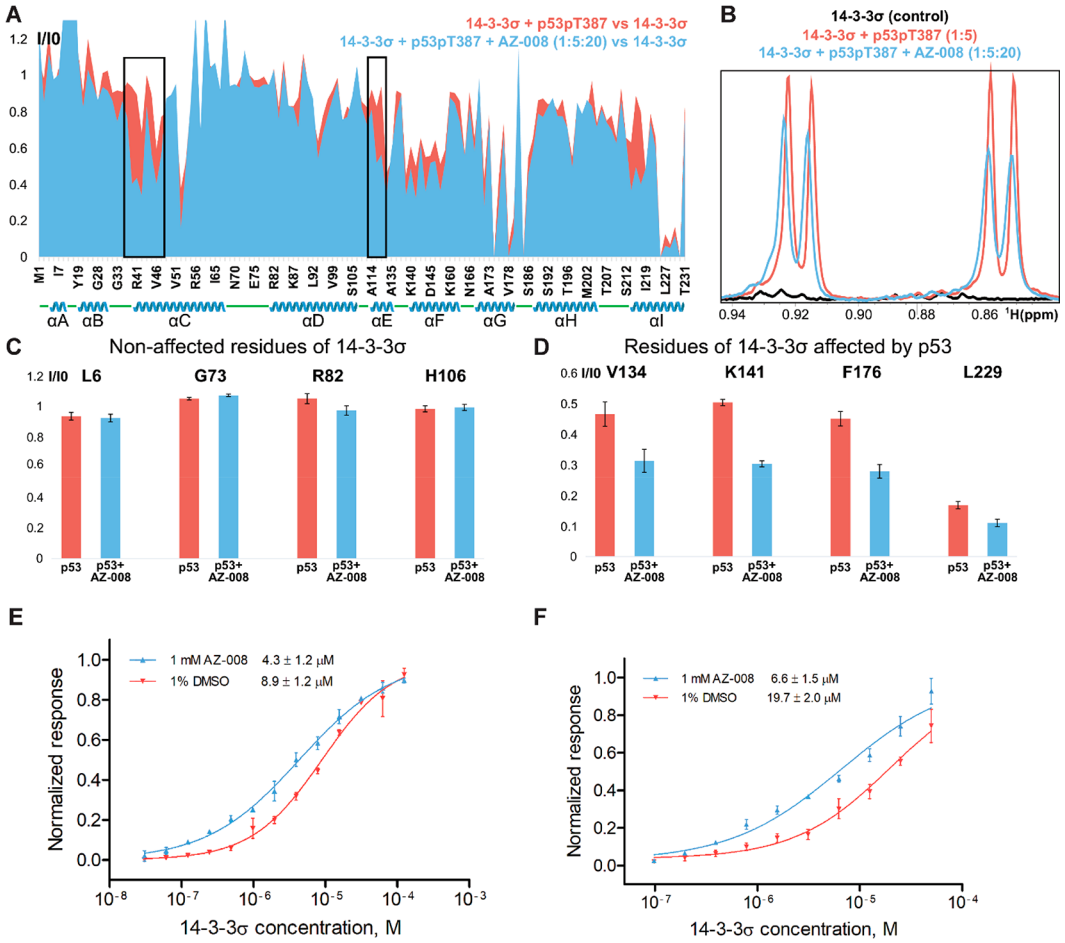

Figure 5. AZ-008 stabilizes the 14-3-3σ/p53pT387 complex. (A) Plot of the intensity ratios I/I_0 (y-axis) of corresponding ^{1}H−^{15}N correlation peaks in the 2D 14-3-3σΔC17 spectra of, in red: the peptide-bound 14-3-3σΔC17 (100 μM 14-3-3σ in the presence of 500 μM p53pT387, I) and free 14-3-3σ (100 μM 14-3-3σ I_0); in blue: corresponding to the peptide and fragment-bound 14-3-3σ (100 μM 14-3-3σ with 500 μM p53pT387 and 2000 μM AZ-008, I) and free 14-3-3σ (100 μM 14-3-3σ, I_0) protein. Note that the boxed regions correspond to the same areas affected in Figure 4 D and therefore show that the binding site of the fragment is the same when the peptide is present or not. (B) ^{1}H NMR signals of the spectrum of 100 μM 14-3-3σ (in black), 100 μM 14-3-3σ in the presence of 500 μM p53pT387 (in red), and 100 μM 14-3-3σ in the simultaneous presence of 500 μM p53pT387 and 2000 μM AZ-008 (in blue). The NMR signals correspond to the Hδ protons of L383 of the p53pT387 peptide. CSP in the peptide signals can be observed when AZ-008 is added to the solution containing the 14-3-3σ/p53pT387 complex. (C,D) Plot of the ratios of the bound (I)/free (I_0) ^{1}H−^{15}N TROSY-HSQC correlation peak intensities of individual resonances corresponding to residues of 100 μM 14-3-3σ, remote from the interaction site (C) or close to the p53pT387 interaction site of (D), in the presence of 500 μM p53pT387 (in red) and 100 μM 14-3-3σ in the simultaneous presence of 500 μM p53pT387 and 2000 μM AZ-008 (in blue). Error bars of I/I_0 ratios were calculated based on the maximum noise estimate of each spectrum. Note that the resonances corresponding to regions affected by the p53pT387 peptide binding were considerably more affected in the presence of AZ-008. (E) Titration of 14-3-3σ to a fluorescently labeled p53pT387 peptide in the absence and presence of 1 mM of AZ-008. Shown are average and standard deviation of three independent experiments. (F) SPR measurement of 14-3-3σ binding to immobilized p53pT387 peptide in the absence and presence of 1 mM AZ-008. Shown are average and standard deviation of three independent experiments.

interaction between 14-3-3σ and a p53pT387 peptide (32mer) containing the complete C-terminal domain. The enthalpically favorable contact between the amino substituent of AZ-008 and E388 of p53pT387 observed in the docking complex described above helps to explain the observed effect. Although this effect is objectively small, it appears to be tangible as it was confirmed quantitatively by two separate methods, but also qualitatively by NMR. Moreover, the 2-fold effect observed here is in accordance with the change in activity that small, noncovalent molecular fragments are expected to induce. Most importantly, these results hint at the possibility of transforming inactive fragments initially identified in X-ray crystallography and/or NMR studies into active molecules through rational design of structural extensions.

DISCUSSION AND CONCLUSIONS

Targeted stabilization of PPIs is an underexplored concept in drug discovery despite numerous examples from natural products and synthetic molecules advocating for this principal strategy.[2,3,30] Successful drugs that operate by stabilizing PPIs have almost exclusively only been recognized as PPI stabilizers after their therapeutic relevance was shown and in many cases even long after FDA approval. One famous example of such drugs is thalidomide and its derivatives, for example, lenalidomide,[31] which are collectively called IMiDs (immunomodulatory drugs). Lenalidomide acts as a "molecular glue" that hijacks a ubiquitin ligase for the targeted degradation of a neosubstrate protein.[32] Another example is the history of the immunosuppressants rapamycin and FK506 which puzzled the

https://dx.doi.org/10.1021/acs.jmedchem.9b01942
J. Med. Chem. 2020, 63, 6694−6707

community for a long time, how these natural products actually convey their therapeutic effect. Eventually it was shown that although they initially bind to the same primary receptor protein, FKBP12, their actual functional targets are the phosphatase calcineurin (FK506) and the protein kinase mTOR (rapamycin) that were "glued" to FKBP12 by the natural products and thus inactivated.[33,34]

A third, recent success story of the PPI induction and stabilization concept is proteolysis targeting chimeras (PROTACs), a technology employing heterobifunctional small molecules that facilitate the interaction of a target protein with a ubiquitin E3 ligase.[35] This approach has not only attracted a lot of attention in the chemical biology field but is currently explored by many pharma companies and at least half a dozen start-up companies. Together with the aforementioned, rather serendipity-driven success examples of IMiDs and "molecular glue" natural products, PROTACs may define a new conceptional era of pharmacologic intervention where an enhancement or induction of a native regulatory process (targeted protein degradation) instead of a direct protein inhibition is the underlying principle.

Our approach to enhance the regulatory function of 14-3-3 PPIs with different partners like p53 or TAZ is an innovative extension of this concept with the added advantage that a physiological, already implemented regulatory network is addressed with small molecules and also that function-enhancing PPIs, as in the case of 14-3-3/p53, can be promoted. We and others have shown in the past that especially the natural product class of the fusicoccanes can be employed as orthosteric stabilizers of 14-3-3 PPIs.[7,11,21,22,26,36−39] However, with only supramolecular ligands[40,41] that are hard to trace by medicinal chemistry, and two screening hits of 14-3-3 PPIs,[27,42] there is a clear need to expand the chemical diversity of 14-3-3 PPI stabilizers. A very useful approach to achieve this goal is fragment-based drug discovery (FBDD).[28] We have shown that fragments binding to 14-3-3 protein complexes can be identified[43,44] and in particular covalent fragment discovery is a fruitful approach,[45] as can be seen in the context of the current work, too (Figure 3 and SI, Figure S15). Especially in the new field of targeting rim-of-the interface pockets with orthosteric stabilizers, FBDD is extremely valuable because it circumvents the bias of traditional compound collections used for high throughput-screening and allows to efficiently probe the chemical space to identify starting points for the development of PPI stabilizers. However, one potential drawback of FBDD in regards to the discovery of PPI stabilizers might be that most identified fragments are silent in classical biophysical assays used for high-throughput screening, as perfectly exemplified within this study. X-ray crystallography and NMR studies therefore appear as the methods of choice, to first find fragment scaffolds capable of binding to the target protein(s), and then develop their activities, a goal that has not yet been successfully accomplished and that represents a considerable challenge.

As our example has shown, specificity for two different, but closely related PPI interfaces can be aimed for even at the very early stage of extending an initial fragment hit. Through a relatively limited series of protein X-ray crystallography identified fragments (see also SI, Figures S16−S34) we were able to identify promising chemical starting points for the future development of active stabilizers that discriminate between the 14-3-3 complexes with p53pT387 and TAZpS89. This is important for the prospect to make the widespread 14-3-3 interactome accessible for drug discovery but also bears implications for other PPIs. An analysis by the Skolnick group has shown that in the crystal structures of 1,611 protein−protein complexes, the majority of "ligandable" pockets are located with a 6 Å distance from the protein interfaces,[46] which is well exemplified by the fragment-binding site of our study. This area, possibly privileged for small-molecule accommodation, is the region where orthosteric PPI stabilizers are supposed to bind. Together with the overall high structural diversity of PPI interfaces this observation nourishes the prospect that for many regulatory protein complexes a specific, rim-of-the interface targeting, orthosteric stabilizer might be developed.

EXPERIMENTAL SECTION

Peptide Synthesis. FITC labeled and acetylated 13mer TAZpS89 were synthesized via Fmoc solid-phase peptide synthesis (SPPS) using an automated Intavis MultiPepRSi peptide synthesizer and a rink amide AM resin (Novabiochem; 0.59 mmol/g loading). The peptides used for NMR measurements and for crystallization studies were acetylated at the N terminus (1:1:3 Ac2O/pyridine/NMP) before resin cleavage. The peptides used for FP assays were manually labeled with FITC (Sigma-Aldrich) attached to a β-alanine linker introduced via Fmoc-β-Ala-OH (Iris Biotech) under standard SPPS conditions. All peptides were purified by preparative reversed-phase HPLC with MS detection. TAMRA labeled 32-mer p53 peptide and acetylated 12-mer p53 were commercially synthesized by Anaspec and Caslo, respectively.

14-3-3 Expression. His_6-tagged 14-3-3σ full-length and ΔC (truncated after T231; for crystallography) were expressed in BL21(DE3) competent cells with a pPROEX HTb plasmid and purified with a nickel column. The His_6-tag was cleaved off using TEV protease, and a second purification was performed by size-exclusion chromatography (Superdex75). The proteins were dialyzed against FP or crystallization buffers before use.

Crystallography. 14-3-3$\sigma\Delta$C/TAZpS89 crystals: 14-3-3$\sigma\Delta$C and acetylated TAZpS89 peptide, both in crystallization buffer (25 mM HEPES pH 7.5, 100 mM NaCl, 10 mM $MgCl_2$ and 2 mM β-mercaptoethanol), were combined in a 1:2 14-3-3$\sigma\Delta$c/TAZpS89 molar ratio with a final protein concentration of 12 mg/mL. After overnight complexation, hanging-drop crystallization wells were setup using a 1:1 ratio of precipitation buffer (95 mM HEPES pH 7.1, 0.19 M $CaCl_2$, 5% glycerol, and 27% PEG400) and complexation mixture for a total drop volume of 2 μL. Crystals were grown within 10 days at 4 °C.

14-3-3$\sigma\Delta$C/p53pT387 crystals: 14-3-3$\sigma\Delta$c and acetylated p53pT387 peptide, both in crystallization buffer (25 mM HEPES pH 7.5, 100 mM NaCl, 10 mM $MgCl_2$, and 2 mM β-mercaptoethanol), were combined in a 1:2 14-3-3$\sigma\Delta$c/TAZ molar ratio with a final protein concentration of 12 mg/mL. After overnight complexation, hanging-drop crystallization wells were setup using a 1:1 ratio of precipitation buffer (0.1 M HEPES pH 7.5, 0.2 M $CaCl_2$, 5% glycerol, 2 mM β-mercaptoethanol, and 28% PEG400) and complexation mixture for a total drop volume of 2 μL. Crystals were grown within 10 days at 4 °C.

The compounds screened were part of the X-ray crystallography subset of the AstraZeneca fragments collection. Fragment soaking was performed on crystals of 10 days and older by adding 0.2 μL of a 100 mM stock solution in dimethyl sulfoxide to the 2 μL drop for a final concentration of 20 mM. Crystals were fished after a minimum of 2 days and flash-cooled in liquid nitrogen.

Data sets were collected either on an in-house Rigaku Micromax-003 (Rigaku Europe, Kemsing Sevenoaks, UK) sealed tube X-ray source and a Dectris Pilatus 200 K detector (DECTRIS Ltd., Baden-Daettwil, Switzerland) or at the DESY PETRA III synchrotron beamline P11 (DESY, Hamburg, Germany). All data sets were indexed, integrated, and scaled using either iMosflm or DIALS

https://dx.doi.org/10.1021/acs.jmedchem.9b01942
J. Med. Chem. 2020, 63, 6694−6707

followed by AIMLESS. Phasing was performed using molecular replacement in Molrep using PDBs 5N75 (14-3-3σ/TAZ) or 5MHC (14-3-3σ/p53) as search model. Phaser, Coot, and phenix.refine were thereafter used in alternating cycles of model building and refinement.

Production of $^{15}N^{2}H$ Labeled 14-3-3σΔC for NMR Spectroscopy. The $^{15}N^{2}H$ labeled 14-3-3σ (ΔC, cleaved after T231) for NMR studies was expressed in *Echerichia coli* BL21 (DE3) cells transformed with a pProExHtb vector carrying the cDNA to expres,s an N-terminally His_6-tagged human 14-3-3σ. Briefly, the cells were grown in 1 L of deuterated M9 minimal medium supplemented with 2 g/L $^{12}C_6{}^{2}H_7$ glucose, 1 g/L ^{15}N ammonium chloride, 0.4 g/L Isogro $^{15}N^{12}C^{2}H$ Powder Growth Medium (Sigma-Aldrich), and 100 μg/mL ampicillin and the recombinant protein was then purified by affinity chromatography using a Ni-NTA column (GE Healthcare). The His_6-tag was further cleaved by the TEV protease and the protein was further dialyzed overnight at 4 °C against NMR buffer (100 mM sodium phosphate, pH 6.8, 50 mM NaCl), concentrated, aliquoted, flash frozen, and stored at −80 °C. A detailed protocol can be found at.[29]

$^{15}N-^{1}H$ TROSY-HSQC NMR Spectroscopy. $^{1}H-^{15}N$ transverse relaxation optimized spectroscopy-heteronuclear single quantum coherence spectroscopy (TROSY-HSQC) spectra were acquired in 3 mm tubes (sample volume 200 μL) using a 900 MHz Bruker Avance Neo spectrometer, equipped with a cryoprobe. The spectra were recorded at 32 °C, in a buffer containing 100 mM sodium phosphate, 50 mM NaCl, pH 6.8, 4% (v/v) DMSO-d_6, 1 mM DTT, EDTA-free protease inhibitor cocktail (Roche, Basel, Switzerland), and 10% (v/v) D_2O. The experiments were recorded with 3072 complex data points in the direct dimension and 128 complex data points in the indirect dimension, with 184 scans per increment. For the evaluation of the binding of AZ-008 to the 14-3-3σ/p53 complex, spectra of $^{15}N^{2}H$ labeled 14-3-3σΔC 100 μM were recorded in the presence and absence of 2000 μM AZ-008, 500 μM p53pT387 peptide, and simultaneously 500 μM p53pT387 peptide and 2000 μM AZ-008. For the evaluation of the binding of AZ-003 to the 14-3-3σ/TAZ complex, spectra of $^{15}N^{2}H$ labeled 14-3-3σ 100 μM were recorded in the presence and absence of 2000 μM AZ-003, 125 μM TAZpS89 peptide, and simultaneously 125 μM TAZpS89 peptide and 2000 μM AZ-003. Assignments of the backbone resonances of $^{15}N^{2}H$ labeled 14-3-3σΔC were previously reported.[29] A ^{1}H spectrum with water-suppression was additionally recorded for each sample for monitoring the peptide signals. The reference for the ^{1}H chemical shift was relative to 4,4-dimethyl-4-silapentane-1-sulfonic acid (DSS) while ^{15}N chemical shift values were referenced indirectly. Spectra were collected and processed with Topspin 4.0 (Bruker Biospin, Karlsruhe, Germany) and analyzed with Sparky 3.12 (T. D. Goddard and D. G. Kneller, SPARKY 3, University of California, San Francisco). CSPs verified as chemical shift positions (in ppm) on the $^{1}H-^{15}N$ TROSY-HSQC were calculated using the following equation:

$$\Delta\delta = \sqrt{\Delta\delta(^{1}H)^{2} + [0.14 \times \Delta\delta(^{15}N)^{2}]}$$

WaterLOGSY NMR Experiments. WaterLOGSY spectra were acquired in 5 mm tubes (sample volume 530 μL) using a 600 MHz Bruker Avance I spectrometer equipped with a CPQCI cryogenic probe. The spectra were recorded with 32 768 complex data points, with 1024 scans per increment and with a mixing time of 1.7 s (acquisition time of 94 min). The spectra were acquired at 16 °C in a buffer containing 100 mM sodium phosphate, 50 mM NaCl, pH 6.8, and 10% (v/v) D_2O. The final concentration of DMSO-d_6 was 2% (v/v) and was kept constant for all the experiments. For the evaluation of the binding of AZ-008 to the 14-3-3σ/p53 complex, WaterLOGSY spectra were recorded on solutions containing 14-3-3σ 25 μM in the presence and absence of 500 μM AZ-008, 50 μM p53pT387 peptide, and simultaneously 50 μM p53pT387 peptide and 500 μM AZ-008. An additional control experiment consisted of the acquisition of a waterLOGSY spectrum in the presence of 500 μM AZ-008 and in the absence of protein and peptide. A ^{1}H spectrum with water-suppression was additionally recorded for each sample. Spectra were collected, processed and analyzed with Topspin 4.0 (Bruker Biospin, Karlsruhe, Germany).

In Silico Docking of AZ-008 in 14-3-3/p53 Complex. Docking experiments of fragments libraries were performed using Schrödinger Drug Discovery suite (Schrödinger Release 2019-1: Schrödinger, LLC, New York, NY, 2019). The Schrödinger protein preparation wizard was used to prepare the crystal structure. Hydrogen atoms were added and possible metal binding states generated. The protonation and tautomeric states of Asp, Glu, Arg, Lys, and His were adjusted to match a pH of 7.5 and possible orientations of Asn and Gln residues were generated. Hydrogen bond sampling with adjustment of active site water molecule orientations was performed using PROPKA. Water molecules with fewer than two hydrogen bonds to nonwaters were deleted. Finally, the protein−ligand complexes were subjected to geometry refinements using the OPLS3 force field in restrained minimizations. The ligands were prepared using LigPrep in the Schrödinger suite. The OPLS3 force field was used in all ligand preparation steps. Possible protonation and ionization states were assigned to each ligand using EpiK at pH 7.5. Possible stereoisomers, tautomeric states, and metal binding sites were generated.

Surface Plasmon Resonance (SPR). SPR analysis was performed using a Biacore 3000 instrument. CTD Thr387 phosphorylated 32-mer peptide of p53 (AnaSpec) was immobilized onto a CMD200 M sensor chip (Xantec Bioanalytics) by using standard NHS/EDC amine-coupling chemistry. Peptide immobilization was carried out at a flow rate of 20 μL/min and protein titration experiments at 10 μL/min. All measurements were conducted at 25 °C in HBSP+ buffer (0.01 M HEPES pH 7.4, 0.15 M NaCl, 0.05% Surfactant P20, 1% DMSO). 14-3-3σ was injected at indicated concentrations in the presence of 1 mM AZ-008 or 1% DMSO control. KD values were obtained by first fitting the non-normalized data using the "log(agonist) vs response (three parameters)" equation of GraphPad Prism, then taking the fitted upper plateau for data normalization, subsequently using the "Sigmoidal dose-response (variable slope)" equation with a constrain to 100% activity.

Fluorescence Polarization (FP) Assay. Fluorescence polarization measurements were conducted in FP-buffer (10 mM HEPES pH 7.4, 150 mM NaCl, 0.01% TWEEN-20, 1.0 mg/mL BSA). *Protein titrations*: dilution series of 14-3-3σ were made in triplet in low binding Corning black round bottom 384-well plates in FP-buffer containing a fixed concentration of labeled 32mer peptide (10 nM TAMRA-p53) and 1% DMSO or 1 mM AZ-008. Plate was incubated at room temperature protected from light for 1 h and polarization was measured using PHERAstar (BMG Labtech) microplate reader (λ_{ex}, 535 nm; λ_{em}, 590 nm). KD values were obtained by first fitting the non-normalized data using the "log(agonist) vs response (three parameters)" equation of GraphPad Prism, then taking the fitted upper plateau for data normalization, subsequently using the "Sigmoidal dose-response (variable slope)" equation with a constrain to 100% activity. *Compound titrations*: dilution series of the fragments dissolved in DMSO were made with fixed concentration of labeled peptides (FITC-TAZpS89:10 nM; TAMRA-p53pT387:10 nM) and protein (40 nM and 10 μM 14-3-3σ for TAZ and p53, respectively) (Control: DMSO concentration 1% v/v). The Corning 384-well plates (black, low volume, low binding, round-bottom) were incubated at 4C protected from light overnight and polarization was measured using Tecan Infinite F500 plate reader (Thermo Fisher) using appropriate excitation and emission wavelength for FITC (λ_{ex}, 485 nm; λ_{em}, 535 nm) and TAMRA (λ_{ex}, 535 nm; λ_{em}, 590 nm)

Synthesis and Characterization of Fragments. *General Chemistry Statement.* All solvents and chemicals used were of reagent grade. Purity and characterization of compounds were established by a combination of LC−MS and NMR techniques. LC-MS spectra were obtained on a Shimadzu UFLC fitted with a Shimadzu LCMS-2020 mass spectrometer and a Waters BEH C18 (50 mm × 2.1 mm, 1.7 μm) or Shim-pack XR-ODS (50 mm × 3.0 mm, 2.2 μm) or Phenomenex Gemini-NX 3μ C18 110A (50 mm × 3.0 mm, 3 μm) column at a flow rate of 1.2 mL/min 95% A to 95% B over 2.0 min with a 0.6 min hold, where A = 0.1% formic acid or

https://dx.doi.org/10.1021/acs.jmedchem.9b01942
J. Med. Chem. 2020, 63, 6694−6707

0.05% TFA in water and B = acetonitrile. Purity was determined by UV absorption at a wavelength of 254 nm, and the mass ion was determined by electrospray ionization (ESI, Micromass Instrument). All final compounds were found to be of 95% purity or greater, as assessed by LC−MS and ^{1}H NMR. ^{1}H NMR spectra were recorded on a 300 or 400 MHz using Bruker spectrometers and using DMSO-d_6, $CDCl_3$, or MeOD-d_4 as solvent depending on solubility. Data for ^{1}H NMR were reported as chemical shifts (in parts per million from internal standard tetramethylsilane), multiplicity (s = singlet, d = doublet, t = triplet, q = quartet, h = heptet, m = multiplet, br = broad) and integration. Preparative high-performance liquid chromatography (HPLC) was performed on a Waters or Phenomenex column using decreasingly polar mixtures of water (containing 1% formic acid or 1% aqueous NH4OH) and acetonitrile. Purification by flash column chromatography (FCC) was typically performed using silica gel (Merck 7734 grade), and solvent mixtures and gradients are recorded herein. All reactions were performed under nitrogen at room temperature (rt) unless otherwise stated.

*Synthesis Pathway to 7-[(2-Amino-1-methyl-ethyl)amino]-benzothiophene-2-carboxamidine (AZ-005) (SI, Scheme S1). Step a: Methyl 7-[[2-(tert-Butoxycarbonylamino)-1-methyl-ethyl]-amino]benzothiophene-2-carboxylate (**1**).* Xantphos (341 mg, 0.59 mmol) and $Pd_2(dba)_3$ (270 mg, 0.30 mmol) were added to Cs_2CO_3 (2884 mg, 8.85 mmol), methyl 7-bromobenzo[*b*]thiophene-2-carboxylate (800 mg, 2.95 mmol), and *tert*-butyl (2-aminopropyl)-carbamate (617 mg, 3.54 mmol) in toluene (20 mL) at 20 °C under nitrogen. The resulting solution was stirred at 130 °C for 4 h. The crude product was purified by flash silica chromatography, elution gradient 0−10% EtOAc in petroleum ether. Pure fractions were evaporated to dryness to afford the title compound (1000 mg, 93%) as a gum. ^{1}H NMR (300 MHz, DMSO-d_6) δ 1.08−1.23 (d, J = 6.3 Hz, 3H), 1.40 (s, 9H), 2.92−3.08 (m, 1H), 3.16−3.31 (m, 1H), 3.62−3.79 (m, 1H), 3.89 (s, 3H), 5.38−5.50 (m, 1H), 6.73−6.84 (m, 1H), 7.03−7.13 (m, 1H), 7.27−7.31 (m, 2H), 8.10 (s, 1H). MS (ESI) $[M + H]^+$ = 365.

*Step b: Methyl 7-[(2-Amino-1-methyl-ethyl)amino]-benzothiophene-2-carboxylate (**2**).* TFA (0.106 mL, 1.37 mmol) was added to methyl 7-((1-((tert-butoxycarbonyl)amino)propan-2-yl)amino)benzo[*b*]thiophene-2-carboxylate (500 mg, 1.37 mmol) in DCM (20 mL) at 20 °C. The resulting solution was stirred at rt for 1 h. The crude product was purified by flash silica chromatography, elution gradient 0−10% MeOH in DCM. Pure fractions were evaporated to dryness to afford the title compound (360 mg, 99%) as a gum. ^{1}H NMR (400 MHz, DMSO-d_6) δ 1.20−1.26 (d, J = 6.4 Hz, 3H), 2.94−3.11 (m, 2H), 3.90 (s, 3H), 3.92−4.01 (m, 1H), 5.35−5.78 (br s, 1H), 6.75−6.81 (d, J = 6.5 Hz, 1H), 7.28−7.40 (m, 2H), 7.87 (s, 2H), 8.13 (s, 1H). MS (ESI) $[M + H]^+$ = 265.

*Step c: 7-[(2-Amino-1-methyl-ethyl)amino]benzothiophene-2-carboxamidine (**AZ-005**).* Methyl 7-((1-aminopropan-2-yl)amino)-benzo[*b*]thiophene-2-carboxylate (300 mg, 1.13 mmol) was added to ammonium chloride (243 mg, 4.54 mmol) and trimethylaluminum (327 mg, 4.54 mmol) in toluene (50 mL) at 20 °C under nitrogen. The resulting solution was stirred at 110 °C for 4 h. The crude product was purified by preparative column: XBridge Prep OBD C18 column 19 mm × 250 mm, 5 μm; mobile phase A, water (0.1%FA); mobile phase B, MeCN; flow rate, 20 mL/min; gradient, 2% B to 30% B. Fractions containing the desired compound were evaporated to dryness to afford the title compound (30.0 mg, 7.72%) as a solid. 1H NMR (400 MHz, methanol-d_4) δ 1.29−1.46 (d, J = 6.4 Hz, 3H), 3.10−3.24 (m, 2H), 4.03−4.17 (m, 1H), 6.89−7.00 (dd, J = 6.7, 1.9 Hz, 1H), 7.39−7.49 (m, 2H), 8.20 (s, 1H), 8.57 (s, 2H). MS (ESI) $[M + H]^+$ = 249.

*Synthesis Pathway to 4-[(2-Amino-1-methyl-ethyl)amino]-6-(sulfanylmethyl)benzothiophene-2-carboxamidine (**AZ-006**) (SI, Scheme S2). Step a: Methyl 4-Bromo-6-methyl-benzothiophene-2-carboxylate.* Methyl 2-mercaptoacetate (2.69 g, 25.34 mmol) was added to 2-bromo-6-fluoro-4-methylbenzaldehyde (5 g, 23.04 mmol) and K_2CO_3 (6.37 g, 46.08 mmol) in DMF (20 mL) at 25 °C. The resulting suspension was stirred at 100 °C for 2 h. The reaction mixture was diluted with EtOAc (250 mL) and washed sequentially with saturated brine (200 mL × 3). The organic layer was dried over Na_2SO_4, filtered, and evaporated to afford the title compound (5.0 g, 76%) as a solid. Taken through to the next step without further purification.

Step b: 4-Bromo-6-methyl-benzothiophene-2-carboxamide. A solution of methyl 4-bromo-6-methylbenzo[*b*]thiophene-2-carboxylate (6.5 g, 22.79 mmol) in NH_3 in MeOH (7 M) (75 mL) was stirred at 110 °C overnight. The mixture was concentrated to obtain the crude product, which was used in next step directly.

*Step c: 4-Bromo-6-methyl-benzothiophene-2-carbonitrile (**3**).* TFA (10.98 mL, 77.74 mmol) was added to a solution of 4-bromo-6-methylbenzo[*b*]thiophene-2-carboxamide (7 g, 25.91 mmol) and pyridine (10.48 mL, 129.56 mmol) in DCM (30 mL). The mixture was stirred at 25 °C for 0.5 h. The reaction mixture was diluted with DCM (200 mL) and washed sequentially with 0.1 M HCl (100 mL × 2). The organic layer was dried over Na_2SO_4, filtered, and evaporated to afford the title compound (6 g) as a solid. Taken through to the next step without further purification.

Step d: 4-Bromo-6-(bromomethyl)benzothiophene-2-carbonitrile. NBS (1.853 g, 10.41 mmol) was added in one portion to 4-bromo-6-methylbenzo[*b*]thiophene-2-carbonitrile (2.5 g, 9.92 mmol) and BPO (0.240 g, 0.99 mmol) in CCl_4 (150 mL) at 90 °C. The resulting solution was stirred at 90 °C for 2 h. The reaction mixture was diluted with EtOAc (200 mL) and washed sequentially with saturated brine (150 mL × 2). The organic layer was dried over Na_2SO_4, filtered, and evaporated to afford crude product. The crude product was purified by flash silica chromatography, elution gradient 0−2% EtOAc in petroleum ether. Pure fractions were evaporated to dryness to afford the title compound (2.70 g, 82%) as a white solid. ^{1}H NMR (300 MHz, DMSO-d_6) δ 4.89 (s, 2H), 7.91 (s, 1H), 8.31 (s, 1H), 8.39 (s, 1H).

*Step e: (4-Bromo-2-cyano-benzothiophen-6-yl)methyl Acetate (**4**).* Silver acetate (1.639 g, 9.82 mmol) was added to 4-bromo-6-(bromomethyl)benzo[*b*]thiophene-2-carbonitrile (2.5 g, 7.55 mmol) in DMF (12 mL) at 20 °C under nitrogen. The resulting mixture was stirred at 60 °C for 1 h. The reaction mixture was filtered through Celite. The crude product was purified by flash C18-chromatography, elution gradient 40−50% MeCN in water. Pure fractions were evaporated to dryness to afford the title compound (2.100 g, 90%) as a solid. ^{1}H NMR (300 MHz, DMSO-d_6) δ 2.13 (s, 3H), 5.23 (s, 2H), 7.82 (s, 1H), 8.22 (s, 1H), 8.38 (s, 1H).

*Step f: [4-[[2-(tert-Butoxycarbonylamino)-1-methyl-ethyl]-amino]-2-cyano-benzothiophen-6-yl]methyl Acetate (**5**).* $Pd_2(dba)_3$ (0.768 g, 0.84 mmol) was added to (4-bromo-2-cyanobenzo[*b*]thiophen-6-yl)methyl acetate (2.6 g, 8.38 mmol), *tert*-butyl (2-aminopropyl)carbamate (1.753 g, 10.06 mmol), Cs_2CO_3 (3.43g,10.52 mmol), and Xantphos (0.970 g, 1.68 mmol) in toluene (25 mL) at 25 °C under nitrogen. The resulting solution was stirred at 130 °C for 3 h. The reaction mixture was filtered using a Buchner funnel, and the solvent was removed under reduced pressure. The crude product was purified by flash silica chromatography, elution gradient 1−10% EtOAc in petroleum ether. Pure fractions were evaporated to dryness to afford the title compound (1.700 g, 50.3%) as a solid. MS (ESI) $[M + H]^+$ = 404.

Step g: tert-Butyl N-[2-[[2-(N-Hydroxycarbamimidoyl)-6-(hydroxymethyl)benzothiophene-4-yl]amino]propyl]carbamate. Hydroxylamine hydrochloride (0.861 g, 12.39 mmol) was added to (4-((1-((*tert*-butoxycarbonyl)amino)propan-2-yl)amino)-2-cyanobenzo[*b*]thiophen-6-yl)methyl acetate (1 g, 2.48 mmol), K_2CO_3 (2.055 g, 14.87 mmol) in MeOH (20 mL) at 25 °C under nitrogen. The resulting solution was stirred at 50 °C for 1 h. The reaction mixture was filtered through Celite. The crude product was purified by flash silica chromatography, elution gradient 0−20% MeOH in DCM. Pure fractions were evaporated to dryness to afford the title compound (0.600 g, 61.4%) as a solid. MS (ESI) $[M + H]^+$ = 395.

Step h: tert-Butyl N-[2-[[2-Carbamimidoyl-6-(hydroxymethyl)-benzothiophen-4-yl]amino]propyl]carbamate. Nickel (0.2 g, 3.41 mmol) was added to *tert*-butyl (2-((2-(*N*-hydroxycarbamimidoyl)-6-(hydroxymethyl)benzo[*b*]thiophen-4-yl)amino)propyl)carbamate (0.6 g, 1.52 mmol) and acetic acid (0.5 mL, 8.73 mmol) in MeOH (15 mL) at 25 °C under nitrogen. The resulting solution was stirred

https://dx.doi.org/10.1021/acs.jmedchem.9b01942
J. Med. Chem. 2020, 63, 6694−6707

at 40 °C for 1 h under an atmosphere of hydrogen. The mixture was filtered through a Celite pad, and the solvent was removed under reduced pressure. The reaction mixture was adjusted to pH 8. The crude product was purified by flash silica chromatography, elution gradient 0−20% MeOH in DCM. Pure fractions were evaporated to dryness to afford the title compound (0.450 g, 78%) as a solid. MS (ESI) $[M + H]^+$ = 379.

*Step i: tert-Butyl N-[4-[[2-(tert-Butoxycarbonylamino)-1-methyl-ethyl]amino]-6-(hydroxymethyl)benzothiophene-2-carboximidoyl]carbamate (**6**).* Boc-anhydride (0.920 mL, 3.96 mmol) was added slowly to *tert*-butyl (2-((2-carbamimidoyl-6-(hydroxymethyl)benzo[*b*]thiophen-4-yl)amino)propyl)carbamate (0.4 g, 1.06 mmol), DMAP (0.129 g, 1.06 mmol) and triethylamine (1.841 mL, 13.21 mmol) in DMF (8 mL) at 0 °C under nitrogen. The resulting solution was stirred at 20 °C for 4 h. The reaction mixture was diluted with EtOAc (100 mL) and washed sequentially with saturated brine (20 mL × 3). The organic layer was dried over Na_2SO_4, filtered, and evaporated to afford crude product. The crude product was purified by flash silica chromatography, elution gradient 0−10% MeOH in DCM. Pure fractions were evaporated to dryness to afford the title compound (0.450 g, 35.6%) as a solid. MS (ESI) $[M + H]^+$ = 479.

Step j: [4-[[2-(tert-Butoxycarbonylamino)-1-methyl-ethyl]amino]-2-(N-tert-butoxycarbonylcarbamimidoyl)benzothiophen-6-yl]methylmethanesulfonate. Ms-Cl (0.078 mL, 1.00 mmol) was added dropwise to *tert*-butyl (2-((2-(*N*-(*tert*-butoxycarbonyl)-carbamimidoyl)-6-(hydroxymethyl)benzo[*b*]thiophen-4-yl)amino)-propyl)carbamate (0.4 g, 0.84 mmol) and triethylamine (0.291 mL, 2.09 mmol) in DCM (25 mL) at 0 °C under nitrogen. The resulting solution was stirred at 20 °C for 30 min. The reaction mixture was diluted with DCM (100 mL) and washed sequentially with saturated brine (25 mL × 3). The organic layer was dried over Na_2SO_4, filtered, and evaporated to afford crude product. This was used in the next step directly without further purification.

Step k: S-[[4-[[2-(tert-Butoxycarbonylamino)-1-methyl-ethyl]amino]-2-(N-tert-butoxycarbonylcarbamimidoyl)benzothiophen-6-yl]methyl]ethanethioate. Potassium thioacetate (0.164 g, 1.44 mmol) was added to (4-((1-((*tert*-butoxycarbonyl)amino)propan-2-yl)amino)-2-(*N*-(*tert*-butoxycarbonyl)carbamimidoyl)benzo[*b*]-thiophen-6-yl)methylmethanesulfonate (0.4 g, 0.72 mmol) in DMF (10 mL) at 20 °C under nitrogen. The resulting solution was stirred at 20 °C for 1 h. The reaction mixture was diluted with EtOAc (100 mL) and washed sequentially with saturated brine (20 mL × 3). The organic layer was dried over Na_2SO_4, filtered, and evaporated to afford crude product. The crude product was purified by flash silica chromatography, elution gradient 0−10% MeOH in DCM. Pure fractions were evaporated to dryness to afford the title compound (0.180 g, 46.7%) as a gum. ^{1}H NMR (300 MHz, methanol-d_4) δ 0.85−1.05 (2 H, m), 1.24−1.35 (4 H, m), 1.42 (s, 9 H), 1.56 (9 H, s), 2.34−2.37 (m, 3 H), 4.19 (2 H, s), 6.54 (1 H, s), 7.08 (1 H, s), 8.17 (s, 1H). MS (ESI) $[M + H]^+$ = 537.5.

*Step l: S-[[4-[(2-Amino-1-methyl-ethyl)amino]-2-carbamimidoyl-benzothiophen-6-yl]methyl] ethanethioate (**7**).* TFA (2 mL, 25.96 mmol) was added dropwise to *S*-((4-((1-((*tert*-butoxycarbonyl)amino)propan-2-yl)amino)-2-(*N*-(*tert*-butoxycarbonyl)carbamimidoyl)benzo[*b*]thiophen-6-yl)methyl) ethanethioate (0.15 g, 0.28 mmol) in DCM (6 mL) at 20 °C under nitrogen. The resulting solution was stirred at 20 °C for 2 h. The mixture was concentrated in vacuo, and the crude product was used in the next step directly without further purification.

Step m: 4-[(2-Amino-1-methyl-ethyl)amino]-6-[[[4-[(2-amino-1-methyl-ethyl)amino]-2-carbamimidoyl-benzothiophen-6-yl]-methyldisulfanyl]methyl]benzothiophene-2-carboxamidine. K_2CO_3 (0.411 g, 2.97 mmol) was added to *S*-((4-((1-aminopropan-2-yl)amino)-2-carbamimidoylbenzo[*b*]thiophen-6-yl)methyl) ethanethioate (0.2 g, 0.59 mmol) in MeOH (5 mL) at 20 °C under nitrogen. The resulting solution was stirred at 20 °C for 1 h. The crude product was purified by preparative HPLC (Column: Xselect CSH OBD column 30 mm × 150 mm, 5 μm; mobile phase A, water (0.05%TFA); mobile phase B, MeCN; flow rate, 60 mL/min. Fractions containing the desired compound were evaporated to dryness to afford the title compound (0.025 g, 12.50%) as a solid. ^{1}H NMR (300 MHz, DMSO-d_6) δ 1.22−1.31 (d, J = 6.3, 6H), 2.99−3.08 (d, J = 6.0, 4H), 3.90−4.00 (m, 6H), 6.58 (s, 2H), 7.20 (s, 2H), 8.58 (s, 2H). MS (ESI) $[M + H]^+$ = 587.5.

*Step n: 4-[(2-Amino-1-methyl-ethyl)amino]-6-(sulfanylmethyl)-benzothiophene-2-carboxamidine (**AZ-006**).* Trimethylphosphane in THF (1M, 0.1 mL, 0.10 mmol) was added in one portion to 6,6′-(disulfanediylbis(methylene))bis(4-((1-aminopropan-2-yl)amino)-benzo[*b*]thiophene-2-carboximidamide) (20 mg, 0.03 mmol) in THF (2 mL) and water (0.2 mL) at 20 °C under nitrogen. The resulting solution was stirred at 20 °C for 30 min. The crude product was purified by preparative HPLC (Column: XBridge Prep OBD C18 column 19 mm × 250 mm, 5 μm; mobile phase A, water (0.05% TFA); mobile phase B, MeCN; flow rate, 20 mL/min. Fractions containing the desired compound were evaporated to dryness to afford the title compound (4.00 mg, 26.2%) as a solid. ^{1}H NMR (300 MHz, DMSO-d_6) δ 1.23−1.32 (d, J = 6.4, 3H), 2.97−3.05 (d, J = 6.4, 2H), 3.78 (s, 2H), 3.90−3.99 (m, 1H), 6.62 (s, 1H), 7.28 (s, 1H), 8.50 (s, 1H). MS (ESI) $[M + H]^+$ = 295.

*Synthesis Pathway to 5-(1H-Imidazol-4-yl)-4-phenyl-thiophene-2-carboxamidine (**AZ-007**) (SI, Scheme S3). Step a: Methyl 5-Bromo-4-phenyl-thiophene-2-carboxylate (**8**).* NBS (1.305 g, 7.33 mmol) was added to methyl 4-phenylthiophene-2-carboxylate (1.600 g, 7.33 mmol) in DMF (5 mL) at 25 °C. The resulting solution was stirred at 50 °C for 4 h. The crude product was purified by flash C18-flash chromatography, elution gradient 0−50% MeCN in water. Pure fractions were evaporated to dryness to afford the title compound (1.600 g, 73.5%) as a solid. MS (ESI) $[M + H]^+$ = 297/299.

*Step b: Methyl 4-Phenyl-5-[1-(2-trimethylsilylethoxymethyl)-imidazol-4-yl]thiophene-2-carboxylate (**9**).* A solution of Na_2CO_3 (490 mg, 4.63 mmol) in water (1.000 mL) was added to a stirred suspension of methyl 5-bromo-4-phenylthiophene-2-carboxylate (500 mg, 1.68 mmol), 4-(4,4,5,5-tetramethyl-1,3,2-dioxaborolan-2-yl)-1-((2-(trimethylsilyl)ethoxy)methyl)-1*H*-imidazole (**16**) (500 mg, 1.54 mmol) and $Pd(Ph_3P)_4$ (178 mg, 0.15 mmol) in 1,4-dioxane (5 mL) at 25 °C under nitrogen. The resulting suspension was stirred at 90 °C overnight. The reaction mixture was diluted with EtOAc (200 mL), and washed sequentially with saturated brine (100 mL × 3). The organic layer was dried over Na_2SO_4, filtered, and evaporated to afford crude product. The crude product was purified by flash C18-flash chromatography, elution gradient 0−60% MeCN in water. Pure fractions were evaporated to dryness to afford the title compound (300 mg, 46.9%) as an oil. MS (ESI) $[M + H]^+$ = 415.

*Step c: Methyl 5-(1H-Imidazol-4-yl)-4-phenyl-thiophene-2-carboxylate (**10**).* HCl (1 mL, 32.91 mmol) was added to methyl 4-phenyl-5-(1-((2-(trimethylsilyl)ethoxy)methyl)-1,4,3,2-imidazol-4-yl)thiophene-2-carboxylate (200 mg, 0.48 mmol) in MeOH (5 mL) at 25 °C under nitrogen. The resulting solution was stirred at rt overnight. The solvent was removed under reduced pressure.The crude product was purified by flash C18-flash chromatography, elution gradient 0−50% MeCN in water. Pure fractions were evaporated to dryness to afford the title compound (80 mg, 58.3%) as an oil. MS (ESI) $[M + H]^+$ = 285.

*Step d: 5-(1H-Imidazol-4-yl)-4-phenyl-thiophene-2-carboxamidine (**AZ-007**).* trimethylaluminum (81 mg, 1.13 mmol) was added to ammonium chloride (60.2 mg, 1.13 mmol) in toluene (3 mL) at 0 °C. The resulting suspension was stirred at rt for 1 h. A solution of methyl 5-(1*H*-imidazol-5-yl)-4-phenylthiophene-2-carboxylate (80 mg, 0.28 mmol) in toluene (3.00 mL) was added dropwise to the reaction at 25 °C under nitrogen. The resulting solution was stirred at 110 °C for 2 h. The reaction mixture was filtered through silica and washed with DCM:MeOH (5:1).The solvent was removed under reduced pressure.The crude product was purified by preparative HPLC (XBridge Prep C18 OBD column, 5 μ silica, 19 mm diameter, 150 mm length), using decreasingly polar mixtures of water (containing 0.1% formic acid) and MeCN as eluents. Fractions containing the desired compound were evaporated to dryness to afford the title compound (15.00 mg, 15.76%) as a solid. ^{1}H NMR (400 MHz, methanol-d_4) δ 6.65−6.70 (1 H, m), 7.40−7.55 (5 H, m), 7.75 (1 H, s), 7.88 (1 H, s), 8.49 (1 H, br s). MS (ESI) $[M + H]^+$ = 269.

https://dx.doi.org/10.1021/acs.jmedchem.9b01942
J. Med. Chem. 2020, 63, 6694−6707

*Trimethyl-[2-[[4-(4,4,5,5-tetramethyl-1,3,2-dioxaborolan-2-yl)-imidazol-1-yl]methoxy]ethyl]silane (**16**).* *Step a.* NaH (150 mg, 3.74 mmol) was added slowly to 5-bromo-1*H*-imidazole (500 mg, 3.40 mmol) in THF (10 mL) at 0 °C under nitrogen. The resulting suspension was stirred at rt for 1 h. (2-(Chloromethoxy)ethyl)-trimethylsilane (681 mg, 4.08 mmol) was added dropwise to the reaction at 0 °C over a period of 5 min under nitrogen. The resulting suspension was stirred at rt for 1 h. The reaction mixture was concentrated and diluted with EtOAc (250 mL) and washed sequentially with saturated brine (150 mL × 3). The organic layer was dried over Na_2SO_4, filtered, and evaporated to afford crude product. The crude product was purified by flash C18-flash chromatography, elution gradient 0−50% MeCN in water. Pure fractions were evaporated to dryness to afford 5-bromo-1-((2-(trimethylsilyl)ethoxy)methyl)-1*H*-imidazole (900 mg, 95%) as a colorless oil. MS (ESI) $[M + H]^+ = 277$. *m/z* (ES+), $[M + H]^+ = 277$; acid, HPLC $t_R = 1.114$ min.

Step b. $PdCl_2(dppf)-CH_2Cl_2$ adduct (14.73 mg, 0.02 mmol) was added to 4-bromo-1-((2-(trimethylsilyl)ethoxy)methyl)-1*H*-imidazole (500 mg, 1.80 mmol), 4,4,4′,4′,5,5,5′,5′-octamethyl-2,2′-bi-(1,3,2-dioxaborolane) (916 mg, 3.61 mmol) and potassium acetate (354 mg, 3.61 mmol) in 1,4-dioxane (5 mL) at 25 °C under nitrogen. The resulting suspension was stirred at 90 °C overnight. The reaction mixture was filtered through silica and afforded the title compound. The product was used in the next step without further purification.

*Synthesis Pathway to N-(2-Aminoethyl)-2-carbamimidoyl-7-isopropoxy-benzothiophene-4-carboxamide (**AZ-008**) (SI, Scheme S4).* *Step a: 6-Bromo-3-[(dimethyl-λ^3-oxidanyl)methyl]-2-fluoro-benzaldehyde (**11**).* BuLi (2.5M, 32.4 mL, 81.09 mmol) was added dropwise to diisopropylamine (7.81 g, 77.23 mmol) in THF (200 mL) at −78 °C under nitrogen. The resulting solution was stirred at −20 °C for 40 min. The reaction was incomplete and further 4-bromo-2-fluoro-1-isopropoxybenzene (18 g, 77.23 mmol) was added at −78 °C and the solution was stirred at −78 °C for a further 40 min. The reaction was incomplete and DMF (6 mL, 77.49 mmol) was added and the mixture was stirred at −78 °C for a further 1 h. The reaction mixture was quenched with saturated NH_4Cl (20 mL), extracted with EtOAc (250 mL × 3), and the organic layer was dried over Na_2SO_4, filtered, and evaporated to afford colorless oil. The crude product was purified by flash silica chromatography, elution gradient 0−5% EtOAc in petroleum ether. Pure fractions were evaporated to dryness to afford the title compound (18.90 g, 94%) as a solid. ^{1}H NMR (300 MHz, DMSO-d_6) δ 1.17−1.43 (d, *J* 6.0, 6H), 4.60−4.79 (m, 1H), 7.38−7.58 (m, 2H), 10.17 (s, 1H).

Step b: Methyl 4-Bromo-7-isopropoxy-benzothiophene-2-carboxylate. Methyl 2-mercaptoacetate (8.07 g, 76.01 mmol) was added to 6-bromo-2-fluoro-3-isopropoxybenzaldehyde (18.9 g, 72.39 mmol) and K_2CO_3 (15.01 g, 108.58 mmol) in DMF (60 mL) at 20 °C under nitrogen. The resulting mixture was stirred at 100 °C for 1.5 h. The reaction mixture was diluted with EtOAc (500 mL) and washed sequentially with saturated brine (75 mL × 4). The organic layer was dried over Na_2SO_4, filtered, and evaporated to afford crude product. The crude product was purified by flash silica chromatography, elution gradient 0−10% EtOAc in petroleum ether. Pure fractions were evaporated to dryness to afford the title compound (22.00 g, 92%) as a solid. ^{1}H NMR (300 MHz, DMSO-d_6) δ 1.20−1.40 (d, *J* 6.0, 6H), 3.90 (s, 3H), 4.77−4.92 (m, 1H), 7.05−7.14 (d, *J* 8.5, 1H), 7.59−7.68 (d, *J* 8.4, 1H), 7.92−8.00 (m, 1H).

Step c: 4-Bromo-7-isopropoxy-benzothiophene-2-carboxamide. Methyl 4-bromo-7-isopropoxybenzo[*b*]thiophene-2-carboxylate (3 g, 9.11 mmol) was added to 7 M NH_3 in MeOH (100 mL, 700.00 mmol) at 20 °C under nitrogen. The resulting solution was stirred at 90 °C for 14 h. The solvent was removed under reduced pressure. The product was used in the next step directly without further purification.

*Step d: 4-Bromo-7-isopropoxy-benzothiophene-2-carbonitrile (**12**).* TFA (3.10 mL, 21.96 mmol) was added slowly to 4-bromo-7-isopropoxybenzo[*b*]thiophene-2-carboxamide (2.3 g, 7.32 mmol) and pyridine (2.96 mL, 36.60 mmol) in DCM (150 mL) at 0 °C under nitrogen. The resulting solution was stirred at rt for 1 h. The reaction mixture was diluted with DCM (100) and washed sequentially with 0.1 M HCl (75 mL × 3) and water (50 mL). The organic layer was dried over Na_2SO_4, filtered, and evaporated to the title compound (2.010 g, 93%) as a solid. ^{1}H NMR (300 MHz, DMSO-d_6) δ 1.32−1.41 (d, *J* = 6.0, 6H), 4.82−4.97 (m, 1H), 7.15−7.25 (d, *J* = 8.6, 1H), 7.68−7.77 (d, *J* = 8.4, 1H), 8.32−8.39 (s, 1H).

*Step e: 2-Cyano-7-isopropoxy-benzothiophene-4-carboxylic Acid (**13**).* BuLi in THF (2M, 15.61 mL, 31.22 mmol) was added dropwise to 4-bromo-7-isopropoxybenzo[*b*]thiophene-2-carbonitrile (0.8 g, 2.70 mmol) in THF (50 mL) and dry ice (2.97 mmol, 1.1 equiv) at −78 °C under nitrogen. The resulting solution was stirred at −78 °C for 10 min. The reaction was incomplete, and further dry ice (2.97 mmol) was added in one portion and the solution was stirred at −78 °C for a further 30 min. The reaction mixture was quenched with saturated NH_4Cl (25 mL), extracted with EtOAc (3 × 100 mL), and the organic layer was dried over Na_2SO_4, filtered, and evaporated to afford colorless oil. The crude product was purified by flash silica chromatography, elution gradient 0−10% MeOH in DCM. Pure fractions were evaporated to dryness to afford the title compound (0.550 g, 78%) as a gum. ^{1}H NMR (300 MHz, DMSO-d_6) δ 1.33−1.45 (m, 6H), 4.95−5.09 (m, 1H), 7.21−7.38 (m, 1H), 8.11−8.24 (m, 1H), 8.85 (s, 1H). MS (ESI) $[M - H]^- = 260$.

*Step f: tert-Butyl N-[2-[(2-Cyano-7-isopropoxy-benzothiophene-4-carbonyl)amino]ethyl]carbamate (**14**).* HATU (1.040 g, 2.74 mmol) was added to 2-cyano-7-isopropoxybenzo[*b*]thiophene-4-carboxylic acid (0.55 g, 2.10 mmol), *tert*-butyl (2-aminoethyl)-carbamate (0.405 g, 2.53 mmol), and triethylamine (1.467 mL, 10.52 mmol) in DMF (10 mL) at 20 °C under nitrogen. The resulting solution was stirred at 20 °C for 1 h. The reaction mixture was diluted with EtOAc (100 mL) and washed sequentially with saturated brine (25 mL × 3). The organic layer was dried over Na_2SO_4, filtered, and evaporated to afford crude product. The crude product was purified by flash silica chromatography, elution gradient 0−10% EtOAc in petroleum ether. Pure fractions were evaporated to dryness to afford the title compound (0.350 g, 41.2%) as a solid. ^{1}H NMR (300 MHz, DMSO-d_6) δ 1.33−1.43 (m, 15H), 1.72−1.83 (m, 2H), 3.11−3.22 (m, 2H), 3.56−3.67 (m, 2H), 6.96 (s, 1H), 7.26−7.35 (d, *J* = 8.4, 1H), 7.83−7.93 (d, *J* = 8.3, 1H), 8.71 (s, 1H). MS (ESI) $[M + H]^+ = 404$.

Step g: N-(2-Aminoethyl)-2-cyano-7-isopropoxy-benzothiophene-4-carboxamide. TFA (3 mL, 38.94 mmol) was added to *tert*-butyl (2-(2-cyano-7-isopropoxybenzo[*b*]thiophene-4-carboxamido)ethyl)carbamate (0.35 g, 0.87 mmol) in DCM (12 mL) at 20 °C under nitrogen. The resulting solution was stirred at rt for 1 h. The solvent was removed under reduced pressure. The reaction mixture was adjusted to pH 7. The crude product was purified by flash silica chromatography, elution gradient 0−20% MeOH in DCM. Pure fractions were evaporated to dryness to afford the title compound (0.250 g, 95%) as a solid. ^{1}H NMR (300 MHz, DMSO-d_6) δ 1.33−1.44 (m, 6H), 3.00−3.10 (m, 2H), 3.67−3.98 (m, 2H), 4.88−5.10 (m, 1H), 7.27−7.38 (m, 1H), 7.99−8.11 (m, 2H), 8.78 (s, 1 H). MS (ESI) $[M + H]^+ = 304$.

*Step h: N-(2-Aminoethyl)-2-(N-hydroxycarbamimidoyl)-7-isopropoxy-benzothiophene-4-carboxamide (**15**).* Hydroxylammonium chloride (0.369 g, 5.31 mmol) was added to *N*-(2-aminoethyl)-2-cyano-7-isopropoxybenzo[*b*]thiophene-4-carboxamide (0.23 g, 0.76 mmol) and K_2CO_3 (0.733 g, 5.31 mmol) in MeOH (8 mL) at 25 °C under nitrogen. The resulting solution was stirred at 50 °C for 1 h. The reaction mixture was filtered through Celite. The solvent was removed under reduced pressure to afford the title compound as a solid. The product was used in the next step directly without further purification.

*Step i: N-(2-Aminoethyl)-2-carbamimidoyl-7-isopropoxy-benzothiophene-4-carboxamide (**AZ-008**).* Nickel (0.2 g, 3.41 mmol) was added to *N*-(2-aminoethyl)-2-(*N*-hydroxycarbamimidoyl)-7-isopropoxybenzo[*b*]thiophene-4-carboxamide (0.15 g, 0.45 mmol) and acetic acid (0.5 mL, 8.73 mmol) in MeOH (5 mL) at 25 °C under nitrogen. The resulting solution was stirred at 40 °C for 1 h under an atmosphere of hydrogen. The mixture was filtered through a Celite pad. The solvent was removed under reduced pressure. The

https://dx.doi.org/10.1021/acs.jmedchem.9b01942
J. Med. Chem. 2020, 63, 6694−6707

crude product was purified by preparative HPLC column: Xselect CSH OBD column 30 mm × 150 mm, 5 μm; mobile phase A, water (0.05%TFA), mobile phase B, MeCN; flow rate, 60 mL/min. Fractions containing the desired compound were evaporated to dryness to afford the title compound (0.025 g, 8.67%) as a white solid. ^{1}H NMR (300 MHz, methanol-d_4) δ 1.43−1.52 (d, J = 6.0, 6H), 3.18−3.29 (t, J = 5.9, 2H), 3.65−3.79 (t, J = 6.0, 2H), 4.94−5.04 (m, 1H), 7.14−7.24 (d, J = 8.5, 1H), 7.90−7.99 (d, J = 8.3, 1H), 8.87 (s, 1H). ^{13}C NMR (126 MHz, DMSO-d_6) δ 167.25, 159.88, 158.88, 158.60, 154.39, 138.36, 132.01, 131.91, 130.72, 128.51, 124.14, 108.77, 71.88, 39.05, 22.16. MS (ESI) $[M + H]^+$ = 321. HRMS (ES^+) for $C_{15}H_{21}N_4O_2S$ $[M + H]^+$: calcd 321.1385, found 321.1392.

■ ASSOCIATED CONTENT

Supporting Information

The Supporting Information is available free of charge at https://pubs.acs.org/doi/10.1021/acs.jmedchem.9b01942.

Additional results and X-ray crystallography tables (PDF)

Molecular formula strings (CSV)

PDB docking AZ-008 to p53 (PDB)

Accession Codes

Coordinates and structure factors have been deposited in the Protein Data Bank under the following accession codes. 14-3-3σ/TAZpS89/fragment complexes: 6RHC (AZ-003); 6SLW (AZ-004); 6RJQ (AZ-006); 6SLX (AZ-010); 6RJL (AZ-018); 6RP6 (AZ-019). 14-3-3σ/p53pT387/Fragment complexes: 6S40 (AZ-001); 6RWI (AZ-002); 6RL3 (AZ-003); 6S9Q (AZ-004); 6RX2 (AZ-005); 6R5L (AZ-006); 6RWH (AZ-007); 6RWS (AZ-009); 6RWU (AZ-010); 6SIP (AZ-011); 6SIQ (AZ-012); 6SLV (AZ-013); 6RK8 (AZ-014); 6RJZ (AZ-015); 6RM5 (AZ-016); 6SIO (AZ-017); 6S39 (AZ-018); 6S3C (AZ-019); 6SIN (AZ-020); 6RKK (AZ-21); 6RKM (AZ-022); 6RKI (AZ-023); 6RL6 (AZ-024); 6RL4 (AZ-025); 6RM7 (AZ-026). Authors will release the atomic coordinates and experimental data upon article publication.

■ AUTHOR INFORMATION

Corresponding Authors

Christian Ottmann − *Laboratory of Chemical Biology, Department of Biomedical Engineering and Institute for Complex Molecular Systems, Eindhoven University of Technology, 5600MB Eindhoven, The Netherlands; Department of Organic Chemistry, University of Duisburg-Essen, 47057 Duisburg, Germany;* orcid.org/0000-0001-7315-0315; Phone: +31 40-247-2835; Email: c.ottmann@tue.nl

Isabelle Landrieu − *CNRS ERL9002 Integrative Structural Biology, F-59000 Lille, France; Univ. Lille, Inserm, CHU Lille, Institut Pasteur de Lille, U1167-RID-AGE, Risk Factors and Molecular Determinants of Aging-Related Diseases, F-59000 Lille, France;* orcid.org/0000-0002-4883-2637; Email: isabelle.landrieu@univ-lille.fr

Hongming Chen − *Hit Discovery, Discovery Sciences, Biopharmaceutical R&D, AstraZeneca, Gothenburg, 431 50 Mölndal, Sweden*; Email: hongming.chen71@hotmail.com

Authors

Xavier Guillory − *Laboratory of Chemical Biology, Department of Biomedical Engineering and Institute for Complex Molecular Systems, Eindhoven University of Technology, 5600MB Eindhoven, The Netherlands*

Madita Wolter − *Laboratory of Chemical Biology, Department of Biomedical Engineering and Institute for Complex Molecular Systems, Eindhoven University of Technology, 5600MB Eindhoven, The Netherlands*

Seppe Leysen − *Laboratory of Chemical Biology, Department of Biomedical Engineering and Institute for Complex Molecular Systems, Eindhoven University of Technology, 5600MB Eindhoven, The Netherlands*

João Filipe Neves − *CNRS ERL9002 Integrative Structural Biology, F-59000 Lille, France; Univ. Lille, Inserm, CHU Lille, Institut Pasteur de Lille, U1167-RID-AGE, Risk Factors and Molecular Determinants of Aging-Related Diseases, F-59000 Lille, France*

Ave Kuusk − *Laboratory of Chemical Biology, Department of Biomedical Engineering and Institute for Complex Molecular Systems, Eindhoven University of Technology, 5600MB Eindhoven, The Netherlands; Hit Discovery, Discovery Sciences, Biopharmaceutical R&D, AstraZeneca, Gothenburg, 431 50 Mölndal, Sweden*

Sylvia Genet − *Laboratory of Chemical Biology, Department of Biomedical Engineering and Institute for Complex Molecular Systems, Eindhoven University of Technology, 5600MB Eindhoven, The Netherlands*

Bente Somsen − *Laboratory of Chemical Biology, Department of Biomedical Engineering and Institute for Complex Molecular Systems, Eindhoven University of Technology, 5600MB Eindhoven, The Netherlands*

John Kenneth Morrow − *Department of Pharmaceutical Chemistry and Small Molecule Discovery Center (SMDC), University of California, San Francisco, California 94143, United States*

Emma Rivers − *Hit Discovery, Discovery Sciences, Biopharmaceutical R&D, AstraZeneca, Gothenburg, 431 50 Mölndal, Sweden*

Lotte van Beek − *Laboratory of Chemical Biology, Department of Biomedical Engineering and Institute for Complex Molecular Systems, Eindhoven University of Technology, 5600MB Eindhoven, The Netherlands*

Joe Patel − *Oncology and Discovery Sciences, IMED Biotech Unit, AstraZeneca, Waltham, Massachusetts 02451, United States*

Robert Goodnow − *Oncology and Discovery Sciences, IMED Biotech Unit, AstraZeneca, Waltham, Massachusetts 02451, United States*

Heike Schoenherr − *Oncology and Discovery Sciences, IMED Biotech Unit, AstraZeneca, Waltham, Massachusetts 02451, United States*

Nathan Fuller − *Oncology and Discovery Sciences, IMED Biotech Unit, AstraZeneca, Waltham, Massachusetts 02451, United States*

Qing Cao − *Oncology and Discovery Sciences, IMED Biotech Unit, AstraZeneca, Waltham, Massachusetts 02451, United States*

Richard G. Doveston − *Laboratory of Chemical Biology, Department of Biomedical Engineering and Institute for Complex Molecular Systems, Eindhoven University of Technology, 5600MB Eindhoven, The Netherlands*

Luc Brunsveld − *Laboratory of Chemical Biology, Department of Biomedical Engineering and Institute for Complex Molecular Systems, Eindhoven University of Technology, 5600MB Eindhoven, The Netherlands;* orcid.org/0000-0001-5675-511X

https://dx.doi.org/10.1021/acs.jmedchem.9b01942
J. Med. Chem. 2020, 63, 6694−6707

Michelle R. Arkin − *Department of Pharmaceutical Chemistry and Small Molecule Discovery Center (SMDC), University of California, San Francisco, California 94143, United States;* orcid.org/0000-0002-9366-6770

Paola Castaldi − *Oncology and Discovery Sciences, IMED Biotech Unit, AstraZeneca, Waltham, Massachusetts 02451, United States*

Helen Boyd − *Hit Discovery, Discovery Sciences, Biopharmaceutical R&D, AstraZeneca, Gothenburg, 431 50 Mölndal, Sweden*

Complete contact information is available at: https://pubs.acs.org/10.1021/acs.jmedchem.9b01942

Author Contributions

X.G., M.W., and S.L. contributed equally. The manuscript was written through contributions of all authors. All authors have given approval to the final version of the manuscript.

Notes

The authors declare no competing financial interest.

■ ACKNOWLEDGMENTS

We acknowledge François-Xavier Cantrelle for assistance on NMR data acquisition. The NMR facilities were funded by the Nord Region Council, CNRS, Institut Pasteur de Lille, the European Community (ERDF), the French Ministry of Research, and the University of Lille and by the CTRL CPER, cofunded by the European Union with the European Regional Development Fund (ERDF), by the Hauts de France Regional Council (contract no. 17003781), Métropole Européenne de Lille (contract no. 2016_ESR_05), and French State (contract no. 2017-R3-CTRL phase 1).We acknowledge support for the NMR facilities from TGE RMN THC (CNRS, FR-3050) and FRABio (Univ. Lille, CNRS, FR-3688). The research is supported by funding from the European Union through the AEGIS (H2020-MSCA-ITN-2015, grant no. 67555), and the TASPPI project (H2020-MSCA-ITN-2015, grant no. 675179). J.F.N and I.L acknowledge LabEx (Laboratory of Excellence) for financial support on the scope of the DISTALZ consortium (ANR, ANR-11-LABX-009).

■ ABBREVIATIONS USED

PPI, protein−protein interaction; FBDD, fragment-based drug discovery; FP, fluorescence polarization; SPR, surface plasmon resonance; FDA, Food and Drug Administration; PROTACs, proteolysis targeting chimeras; EtOAc, ethyl acetate; DMSO, dimethyl sulfoxide; DCM, dichloromethane; MeCN, acetonitrile; FA, formic acid; DMF, dimethylformamide; DMAP, 4-dimethylaminopyridine; THF, tetrahydrofuran; TFA, trifluoroacetic acid; NBS, *N*-bromosuccinimide; Ms-Cl, methanesulfonyl chloride; CSP, chemical shift perturbation

■ REFERENCES

(1) Arkin, M. R.; Tang, Y.; Wells, J. A. Small-Molecule Inhibitors of Protein-Protein Interactions: Progressing toward the Reality. *Chem. Biol.* **2014**, *21* (9), 1102−1114.

(2) Bier, D.; Thiel, P.; Briels, J.; Ottmann, C. Stabilization of Protein-Protein Interactions in Chemical Biology and Drug Discovery. *Prog. Biophys. Mol. Biol.* **2015**, *119* (1), 10−19.

(3) Andrei, S. A.; Sijbesma, E.; Hann, M.; Davis, J.; O'Mahony, G.; Perry, M. W. D.; Karawajczyk, A.; Eickhoff, J.; Brunsveld, L.; Doveston, R. G.; Milroy, L.-G.; Ottmann, C. Stabilization of Protein-Protein Interactions in Drug Discovery. *Expert Opin. Drug Discovery* **2017**, *12* (9), 925−940.

(4) Johnson, C.; Crowther, S.; Stafford, M. J.; Campbell, D. G.; Toth, R.; MacKintosh, C. Bioinformatic and Experimental Survey of 14−3-3-Binding Sites. *Biochem. J.* **2010**, *427* (1), 69−78.

(5) Fischer, A.; Baljuls, A.; Reinders, J.; Nekhoroshkova, E.; Sibilski, C.; Metz, R.; Albert, S.; Rajalingam, K.; Hekman, M.; Rapp, U. R. Regulation of RAF Activity by 14−3-3 Proteins: RAF Kinases Associate Functionally with Both Homo- and Heterodimeric Forms of 14−3-3 Proteins. *J. Biol. Chem.* **2009**, *284* (5), 3183−3194.

(6) Molzan, M.; Ottmann, C. Synergistic Binding of the Phosphorylated S233- and S259-Binding Sites of C-RAF to One 14−3-3ζ Dimer. *J. Mol. Biol.* **2012**, *423* (4), 486−495.

(7) Molzan, M.; Kasper, S.; Röglin, L.; Skwarczynska, M.; Sassa, T.; Inoue, T.; Breitenbuecher, F.; Ohkanda, J.; Kato, N.; Schuler, M.; Ottmann, C. Stabilization of Physical RAF/14−3-3 Interaction by Cotylenin A as Treatment Strategy for RAS Mutant Cancers. *ACS Chem. Biol.* **2013**, *8* (9), 1869−1875.

(8) Qureshi, H. Y.; Li, T.; MacDonald, R.; Cho, C. M.; Leclerc, N.; Paudel, H. K. Interaction of 14−3-3ζ with Microtubule-Associated Protein Tau within Alzheimer's Disease Neurofibrillary Tangles. *Biochemistry* **2013**, *52* (37), 6445−6455.

(9) Joo, Y.; Schumacher, B.; Landrieu, I.; Bartel, M.; Smet-Nocca, C.; Jang, A.; Choi, H. S.; Jeon, N. L.; Chang, K.-A.; Kim, H.-S.; Ottmann, C.; Suh, Y.-H. Involvement of 14−3-3 in Tubulin Instability and Impaired Axon Development Is Mediated by Tau. *FASEB J.* **2015**, *29* (10), 4133−4144.

(10) Bozoky, Z.; Krzeminski, M.; Muhandiram, R.; Birtley, J. R.; Al-Zahrani, A.; Thomas, P. J.; Frizzell, R. A.; Ford, R. C.; Forman-Kay, J. D. Regulatory R Region of the CFTR Chloride Channel Is a Dynamic Integrator of Phospho-Dependent Intra- and Intermolecular Interactions. *Proc. Natl. Acad. Sci. U. S. A.* **2013**, *110* (47), E4427−4436.

(11) Stevers, L. M.; Lam, C. V.; Leysen, S. F. R.; Meijer, F. A.; van Scheppingen, D. S.; de Vries, R. M. J. M.; Carlile, G. W.; Milroy, L. G.; Thomas, D. Y.; Brunsveld, L.; Ottmann, C. Characterization and Small-Molecule Stabilization of the Multisite Tandem Binding between 14−3-3 and the R Domain of CFTR. *Proc. Natl. Acad. Sci. U. S. A.* **2016**, *113* (9), E1152−1161.

(12) Chan, S. W.; Lim, C. J.; Guo, K.; Ng, C. P.; Lee, I.; Hunziker, W.; Zeng, Q.; Hong, W. A Role for TAZ in Migration, Invasion, and Tumorigenesis of Breast Cancer Cells. *Cancer Res.* **2008**, *68* (8), 2592−2598.

(13) Yang, H.-Y.; Wen, Y.-Y.; Chen, C.-H.; Lozano, G.; Lee, M.-H. 14−3-3 Sigma Positively Regulates P53 and Suppresses Tumor Growth. *Mol. Cell. Biol.* **2003**, *23* (20), 7096−7107.

(14) Rajagopalan, S.; Sade, R. S.; Townsley, F. M.; Fersht, A. R. Mechanistic Differences in the Transcriptional Activation of P53 by 14−3-3 Isoforms. *Nucleic Acids Res.* **2010**, *38* (3), 893−906.

(15) Rajagopalan, S.; Jaulent, A. M.; Wells, M.; Veprintsev, D. B.; Fersht, A. R. 14−3-3 Activation of DNA Binding of P53 by Enhancing Its Association into Tetramers. *Nucleic Acids Res.* **2008**, *36* (18), 5983−5991.

(16) Saha, M.; Carriere, A.; Cheerathodi, M.; Zhang, X.; Lavoie, G.; Rush, J.; Roux, P. P.; Ballif, B. A. RSK Phosphorylates SOS1 Creating 14−3-3-Docking Sites and Negatively Regulating MAPK Activation. *Biochem. J.* **2012**, *447* (1), 159−166.

(17) Ballone, A.; Centorrino, F.; Wolter, M.; Ottmann, C. Structural Characterization of 14−3-3ζ in Complex with the Human Son of Sevenless Homolog 1 (SOS1). *J. Struct. Biol.* **2018**, *202* (3), 210−215.

(18) Ory, S.; Zhou, M.; Conrads, T. P.; Veenstra, T. D.; Morrison, D. K. Protein Phosphatase 2A Positively Regulates Ras Signaling by Dephosphorylating KSR1 and Raf-1 on Critical 14−3-3 Binding Sites. *Curr. Biol.* **2003**, *13* (16), 1356−1364.

(19) Shen, C.-H.; Yuan, P.; Perez-Lorenzo, R.; Zhang, Y.; Lee, S. X.; Ou, Y.; Asara, J. M.; Cantley, L. C.; Zheng, B. Phosphorylation of BRAF by AMPK Impairs BRAF-KSR1 Association and Cell Proliferation. *Mol. Cell* **2013**, *52* (2), 161−172.

(20) Dumaz, N.; Marais, R. Protein Kinase A Blocks Raf-1 Activity by Stimulating 14−3-3 Binding and Blocking Raf-1 Interaction with Ras. *J. Biol. Chem.* **2003**, *278* (32), 29819−29823.

(21) Liang, X.; Da Paula, A. C.; Bozóky, Z.; Zhang, H.; Bertrand, C. A.; Peters, K. W.; Forman-Kay, J. D.; Frizzell, R. A. Phosphorylation-Dependent 14−3-3 Protein Interactions Regulate CFTR Biogenesis. *Mol. Biol. Cell* **2012**, *23* (6), 996−1009.
(22) Kaplan, A.; Morquette, B.; Kroner, A.; Leong, S.; Madwar, C.; Sanz, R.; Banerjee, S. L.; Antel, J.; Bisson, N.; David, S.; Fournier, A. E. Small-Molecule Stabilization of 14−3-3 Protein-Protein Interactions Stimulates Axon Regeneration. *Neuron* **2017**, *93* (5), 1082.
(23) Ottmann, C.; Marco, S.; Jaspert, N.; Marcon, C.; Schauer, N.; Weyand, M.; Vandermeeren, C.; Duby, G.; Boutry, M.; Wittinghofer, A.; Rigaud, J.-L.; Oecking, C. Structure of a 14−3-3 Coordinated Hexamer of the Plant Plasma Membrane H+ -ATPase by Combining X-Ray Crystallography and Electron Cryomicroscopy. *Mol. Cell* **2007**, *25* (3), 427−440.
(24) Asahi, K.; Honma, Y.; Hazeki, K.; Sassa, T.; Kubohara, Y.; Sakurai, A.; Takahashi, N. Cotylenin A, a Plant-Growth Regulator, Induces the Differentiation in Murine and Human Myeloid Leukemia Cells. *Biochem. Biophys. Res. Commun.* **1997**, *238* (3), 758−763.
(25) Andrei, S. A.; de Vink, P.; Sijbesma, E.; Han, L.; Brunsveld, L.; Kato, N.; Ottmann, C.; Higuchi, Y. Rationally Designed Semi-synthetic Natural Product Analogues for Stabilization of 14−3-3 Protein-Protein Interactions. *Angew. Chem., Int. Ed.* **2018**, *57* (41), 13470−13474.
(26) De Vries-van Leeuwen, I. J.; da Costa Pereira, D.; Flach, K. D.; Piersma, S. R.; Haase, C.; Bier, D.; Yalcin, Z.; Michalides, R.; Feenstra, K. A.; Jiménez, C. R.; de Greef, T. F. A.; Brunsveld, L.; Ottmann, C.; Zwart, W.; de Boer, A. H. Interaction of 14−3-3 Proteins with the Estrogen Receptor Alpha F Domain Provides a Drug Target Interface. *Proc. Natl. Acad. Sci. U. S. A.* **2013**, *110* (22), 8894−8899.
(27) Rose, R.; Erdmann, S.; Bovens, S.; Wolf, A.; Rose, M.; Hennig, S.; Waldmann, H.; Ottmann, C. Identification and Structure of Small-Molecule Stabilizers of 14−3-3 Protein-Protein Interactions. *Angew. Chem., Int. Ed.* **2010**, *49* (24), 4129−4132.
(28) Price, A. J.; Howard, S.; Cons, B. D. Fragment-Based Drug Discovery and Its Application to Challenging Drug Targets. *Essays Biochem.* **2017**, *61* (5), 475−484.
(29) Neves, J. F.; Landrieu, I.; Merzougui, H.; Boll, E.; Hanoulle, X.; Cantrelle, F.-X. Backbone Chemical Shift Assignments of Human 14−3-3σ. *Biomol. NMR Assignments* **2019**, *13* (1), 103−107.
(30) Thiel, P.; Kaiser, M.; Ottmann, C. Small-Molecule Stabilization of Protein-Protein Interactions: An Underestimated Concept in Drug Discovery? *Angew. Chem., Int. Ed.* **2012**, *51* (9), 2012−2018.
(31) Rehman, W.; Arfons, L. M.; Lazarus, H. M. The Rise, Fall and Subsequent Triumph of Thalidomide: Lessons Learned in Drug Development. *Ther. Adv. Hematol.* **2011**, *2* (5), 291−308.
(32) Hughes, S. J.; Ciulli, A. Molecular Recognition of Ternary Complexes: A New Dimension in the Structure-Guided Design of Chemical Degraders. *Essays Biochem.* **2017**, *61* (5), 505−516.
(33) Liu, J.; Farmer, J. D.; Lane, W. S.; Friedman, J.; Weissman, I.; Schreiber, S. L. Calcineurin Is a Common Target of Cyclophilin-Cyclosporin A and FKBP-FK506 Complexes. *Cell* **1991**, *66* (4), 807−815.
(34) Brown, E. J.; Albers, M. W.; Shin, T. B.; Ichikawa, K.; Keith, C. T.; Lane, W. S.; Schreiber, S. L. A Mammalian Protein Targeted by G1-Arresting Rapamycin-Receptor Complex. *Nature* **1994**, *369* (6483), 756−758.
(35) Neklesa, T. K.; Winkler, J. D.; Crews, C. M. Targeted Protein Degradation by PROTACs. *Pharmacol. Ther.* **2017**, *174*, 138−144.
(36) Anders, C.; Higuchi, Y.; Koschinsky, K.; Bartel, M.; Schumacher, B.; Thiel, P.; Nitta, H.; Preisig-Müller, R.; Schlichthörl, G.; Renigunta, V.; Ohkanda, J.; Daut, J.; Kato, N.; Ottmann, C. A Semisynthetic Fusicoccane Stabilizes a Protein-Protein Interaction and Enhances the Expression of K+ Channels at the Cell Surface. *Chem. Biol.* **2013**, *20* (4), 583−593.
(37) Bier, D.; Bartel, M.; Sies, K.; Halbach, S.; Higuchi, Y.; Haranosono, Y.; Brummer, T.; Kato, N.; Ottmann, C. Small-Molecule Stabilization of the 14−3-3/Gab2 Protein-Protein Interaction (PPI) Interface. *ChemMedChem* **2016**, *11* (8), 911−918.
(38) Camoni, L.; Di Lucente, C.; Visconti, S.; Aducci, P. The Phytotoxin Fusicoccin Promotes Platelet Aggregation via 14−3-3-Glycoprotein Ib-IX-V Interaction. *Biochem. J.* **2011**, *436* (2), 429−436.
(39) Paiardini, A.; Aducci, P.; Cervoni, L.; Cutruzzolà, F.; Di Lucente, C.; Janson, G.; Pascarella, S.; Rinaldo, S.; Visconti, S.; Camoni, L. The Phytotoxin Fusicoccin Differently Regulates 14−3-3 Proteins Association to Mode III Targets. *IUBMB Life* **2014**, *66* (1), 52−62.
(40) Bier, D.; Rose, R.; Bravo-Rodriguez, K.; Bartel, M.; Ramirez-Anguita, J. M.; Dutt, S.; Wilch, C.; Klärner, F.-G.; Sanchez-Garcia, E.; Schrader, T.; Ottmann, C. Molecular Tweezers Modulate 14−3-3 Protein-Protein Interactions. *Nat. Chem.* **2013**, *5* (3), 234−239.
(41) Bier, D.; Mittal, S.; Bravo-Rodriguez, K.; Sowislok, A.; Guillory, X.; Briels, J.; Heid, C.; Bartel, M.; Wettig, B.; Brunsveld, L.; Sanchez-Garcia, E.; Schrader, T.; Ottmann, C. The Molecular Tweezer CLR01 Stabilizes a Disordered Protein-Protein Interface. *J. Am. Chem. Soc.* **2017**, *139* (45), 16256−16263.
(42) Richter, A.; Rose, R.; Hedberg, C.; Waldmann, H.; Ottmann, C. An Optimised Small-Molecule Stabiliser of the 14−3-3-PMA2 Protein-Protein Interaction. *Chem. - Eur. J.* **2012**, *18* (21), 6520−6527.
(43) Sijbesma, E.; Skora, L.; Leysen, S.; Brunsveld, L.; Koch, U.; Nussbaumer, P.; Jahnke, W.; Ottmann, C. Identification of Two Secondary Ligand Binding Sites in 14−3-3 Proteins Using Fragment Screening. *Biochemistry* **2017**, *56* (30), 3972−3982.
(44) Valenti, D.; Neves, J. F.; Cantrelle, F.-X.; Hristeva, S.; Lentini Santo, D.; Obšil, T.; Hanoulle, X.; Levy, L. M.; Tzalis, D.; Landrieu, I.; Ottmann, C. Set-up and Screening of a Fragment Library Targeting the 14−3-3 Protein Interface. *MedChemComm* **2019**, *10* (10), 1796−1802.
(45) Sijbesma, E.; Hallenbeck, K. K.; Leysen, S.; de Vink, P. J.; Skóra, L.; Jahnke, W.; Brunsveld, L.; Arkin, M. R.; Ottmann, C. Site-Directed Fragment-Based Screening for the Discovery of Protein-Protein Interaction Stabilizers. *J. Am. Chem. Soc.* **2019**, *141* (8), 3524−3531.
(46) Gao, M.; Skolnick, J. The Distribution of Ligand-Binding Pockets around Protein-Protein Interfaces Suggests a General Mechanism for Pocket Formation. *Proc. Natl. Acad. Sci. U. S. A.* **2012**, *109* (10), 3784−3789.

https://dx.doi.org/10.1021/acs.jmedchem.9b01942
J. Med. Chem. 2020, 63, 6694−6707